Trabajo Fin de Máster
Máster en Ingeniería Industrial

# Thermal Assessment of the JT-60SA Fast-ion Loss Detector (FILD)

Autor: Carlos Cobacho Rodríguez

Tutor: Juan Manuel Ayllón Guerola

Tutor: Manuel García Muñoz

Trabajo Fin de Máster

Máster en Ingeniería Industrial

# Thermal Assessment of the JT-60SA Fast-ion Loss Detector (FILD)

Autor:

Carlos Cobacho Rodríguez

Tutor:

Juan Manuel Ayllón Guerola

Profesor Ayudante Doctor Interino

Tutor:

Manuel García Muñoz

Profesor Titular

Dpto. Ingeniería Mecánica y Fabricación

Escuela Técnica Superior de Ingeniería

Universidad de Sevilla

Sevilla, 2020

Trabajo Fin de Máster:     Thermal Assessment of the JT-60SA Fast-ion Loss Detector (FILD)

Autor:        Carlos Cobacho Rodríguez
Tutor:        Juan Manuel Ayllón Guerola
Tutor:        Manuel García Muñoz

El tribunal nombrado para juzgar el trabajo arriba indicado, compuesto por los siguientes profesores:

Presidente:

Vocal/es:

Secretario:

acuerdan otorgarle la calificación de:

El Secretario del Tribunal

Fecha:

# Agradecimientos

A mis padres, mi hermano y mi familia.

A mi tutor, Juanma, por ayudarme en la realización de este trabajo.

# Resumen

En tanto que las energías renovables y los avances en tecnologías de almacenamiento de energía continúan su camino hacia la transformación del panorama energético mundial, la promesa de una fuente de energía mejor, la energía de fusión, se mantiene siempre sobre el horizonte. Supuestamente, la energía de fusión será casi infinita, limpia y muy segura. Sin embargo, la generación de energía mediante fusión, lo que a menudo se compara con crear un Sol en la Tierra, conlleva muchos retos.

Los reactores de fusión tokamak tienen el diseño más avanzado y llevan siendo desarrollados durante varias décadas. ITER (acrónimo en inglés de Reactor Termonuclear Experimental Internacional) es el tokamak más importante del mundo en estos momentos. Está siendo construido en Francia y debería empezar a operar en 2025. Se espera que ITER sea el punto de inflexión en la generación de energía mediante fusión que físicos, ingenieros y científicos de toda índole llevaban mucho tiempo buscando, al obtener un factor de ganancia Q=10, lo cual significaría que genera diez veces la energía que necesita para operar. Para alcanzar el éxito, muchos otros proyectos llamados satélite trabajan junto a ITER, compartiendo sus avances y descubrimientos. Uno de esos proyectos satélite es JT-60SA (Japón), que no sólo acompañará a ITER durante su desarrollo y operación sino que también ayudará en el desarrollo de los tokamaks del futuro.

En este trabajo estudiaremos el comportamiento térmico de un dispositivo de diagnóstico, FILD (acrónimo en inglés de Detector de Pérdida de Iones Rápidos), que será instalado en el tokamak JT-60SA y cuyo propósito es medir y caracterizar los iones rápidos que se escapan del plasma, y que son en parte responsables de la autosustentación del mismo plasma y de su estabilidad.

Diseñaremos parte de la geometría de FILD y estudiaremos algunos de sus modos de operación con el objetivo en mente de lidiar con los enormes flujos de calor que recibe del plasma, manteniendo siempre un ojo puesto en otras áreas como la del comportamiento mecánico. Contaremos con el bagaje científico y técnico de nuestro equipo, así como de la ayuda de software científico como Ansys Workbench y MATLAB. Diversas optimizaciones y decisiones serán realizadas a lo largo de este trabajo y multitud de interesantes discusiones tendrán lugar para, de este modo, alcanzar nuestros objetivos.

# Abstract

While renewable energies and advances in energy storage technologies continue their road to a global energy transformation, the promise of a better energy source, the fusion energy, remains always on the horizon. Fusion energy is supposed to be almost infinite, clean and very safe. However, fusion energy generation, which is often compared to bringing the Sun down to Earth, carries a lot of challenges.

Tokamak fusion reactors have the most advanced design and have been developed for many decades already. ITER (International Thermonuclear Experimental Reactor) is the most important tokamak in the world at this moment. It is being built in France and is supposed to first operate in 2025. ITER is expected to be the inflection point in the fusion energy generation that physicists, engineers and scientists of all kind have been searching for a long time, attaining a gain factor Q=10, which would mean that it produces ten times as much energy as it requires to operate. In order to succeed, many other satellite projects work together with ITER, sharing their advances and discoveries. One of those satellite projects is JT-60SA (Japan), which will not only accompany ITER during its development and operation but will also help design the tokamaks of the future.

In this work we will study the thermal behaviour of a diagnostic device, FILD (Fast Ion Loss Detector), that is going to be installed in the JT-60SA tokamak and whose purpose is to measure and characterize the fast ions that escape the plasma, which are in part responsible for the self-sustainability of the plasma itself and its stability.

We will design some of the geometry of FILD and study some of its operating modes with the objective in mind of dealing with the huge heat loads it receives from plasma, while keeping an eye at other domains like the mechanical behaviour. We will rely on the scientific and technical background of our team, as well as scientific software such as Ansys Workbench and MATLAB. Many optimizations and choices will be made within this work and plenty of interesting discussions will take place in order to achieve our goals.

# Contents

# 1 Introduction

Generating energy in a clean, sustainable and reliable way is one of the biggest challenges to ever be faced by human society. Energy is used in all its forms and everywhere, whether it is the services sector, transport, households or manufacturing industries (see Figure 1.1).
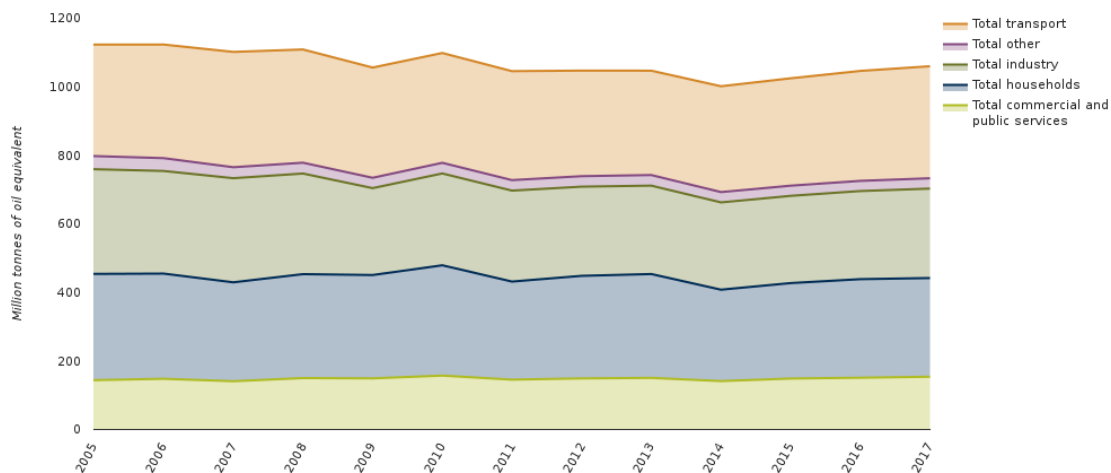


**Figure 1.1** EU's energy consumption evolution by sector in million tonnes of oil equivalent [1].

Such a widespread use of energy requires a huge and complex energy generation infrastructure. Traditionally, governments have mostly relied on fossil energy sources like coal, oil or natural gas, as an engine of progress. However, ecological concerns, the fact that these sources are limited and increasingly expensive as we run out of them, and a rising need of energy independence and equality, have caused a change of paradigm.

Current energetic plans on most developed countries tend to be mainly focused in the following areas:

- The improvement in energy production efficiency:

  This is a never-ending career, maintained by constant technological improvements, allowing us to generate the same amount of energy with fewer resources.

- The improvement in energy usage efficiency:

  Here, it is not only relevant the development of more efficient energy consuming machines, but also the impact of the transport of this energy whether it is through power lines, marine ships, tank trucks or pipelines. By improving these aspects, like, for instance, bringing geographically closer both the

generation and the consuming agents, the amount of energy that society has to generate to carry on with its activities can be reduced.

- A transition to the renewable energy:

  Renewable energy does not produce any waste during its generation and has no operational costs, being the only costs the initial investment and the maintenance costs. It is an unstoppable transformation, lead by the wind and the solar energies that are the ones expanding at a higher rate [2]. This is possible thanks to technological advances and a reduction of their costs added to the expected subsidies for the creation of new plants and the renovation of outdated ones.

Despite the many advantages that renewable energy brings, fossil energy sources remain dominant around the world, as can be seen in Figure 1.2, and it is expected that they will continue coexisting in the future. Furthermore, renewable energy sources are not exempt of drawbacks.

The main disadvantage renewable energy has is its dependency on the weather: solar panels require a minimum amount of radiation intensity to produce energy and, similarly, wind turbines need that wind crosses a certain threshold of speed to start spinning. This variability makes it impossible to rely exclusively on it, at least without a proper energy storage system; although lithium-ion batteries or hydrogen energy storage are very promising technologies, they still need to gain more traction to become decisive [3].
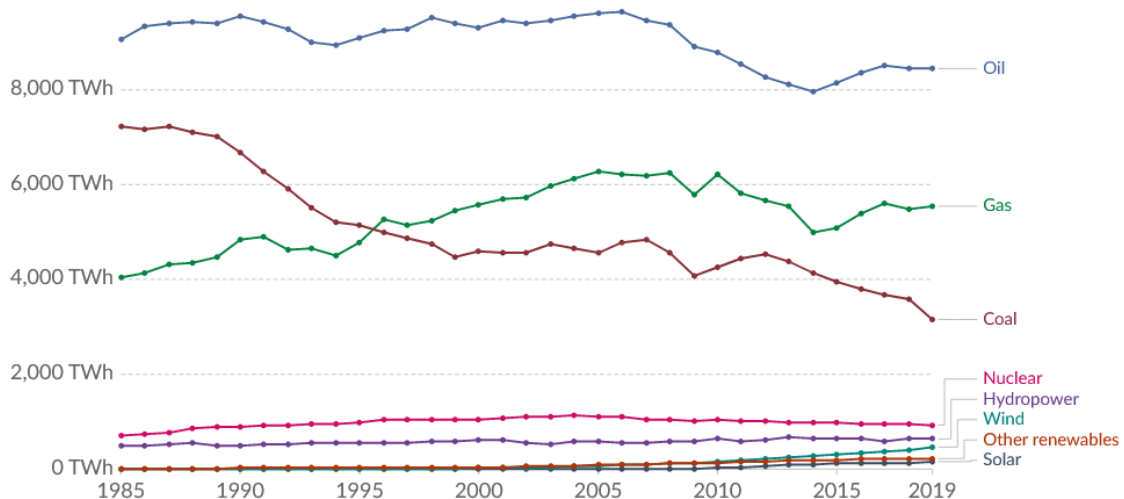


**Figure 1.2** EU's energy consumption evolution by source in TWh [4].

An alternative to fossil and renewable energy sources would be the nuclear fission energy, an energy produced by the separation of the atoms of certain mollecules, like uranium. Nuclear fission reactors have long been operating in many countries and providing an important portion of their global energy supply. Unlike renewable energy sources, their physical principle of operation makes nuclear fission reactors work at a constant rate, providing a consistent amount of energy with negligible power outages. Nevertheless, many countries, backed by public opinion, have stopped building and even have started decommissioning them because of the long lasting radioactive waste they generate and the severe impact that an unlikely nuclear disaster, like the one that occurred in Fukushima in 2011, can produce to humans and the nature.

On the other hand, we have the nuclear fusion energy, an energy naturally produced by stars, like the Sun. Fusion energy is clean and safe, and its waste is far less harmful than the generated in fission reactions as will be later explained in chapter 2. The raw materials that it requires are very common in Earth; hydrogen, for instance, can be considered limitless. Unlike renewable sources, it is completely independent from weather, in fact, it could theorithecally be used anywhere. It looks like fusion energy is the ultimate way of producing energy, but, although the fusion reaction is possible in stars, it is a challenging task to reproduce it in Earth. However, the profit of doing so is enormous: one gram of raw material could produce as much energy as 8

tons of oil [5].

The work presented in this dissertation is about the thermal study and design of the JT-60SA FILD –acronym for Fast Ion Loss Detector–, a diagnostic device currently being designed by the PSFT group (Plasma Science and Fusion Technology, Universidad de Sevilla) for the JT-60SA tokamak. This tokamak is currently being built in Japan and is expected to start operating in 2020.

# 2  Nuclear Fusion

Nuclear physics, and nuclear fusion physics in particular, are vast scientific fields of study. Since the end of the 18th century, when the first, yet unknown, nuclear experiments were performed, scientists have continued discovering new phenomenons and proposing new theories to try to explain the reality around this subject.

Covering the topic of the nuclear fusion as a whole falls outside the scope of this document and is well beyond the knowledge of this author. However, before delving deeper into the main content of this work, we feel the need to explain the basics of the nuclear fusion physics and technology that have brought us to to the study presented in this document.

## 2.1  Nuclear Fusion Reaction

Nuclear fusion is a nuclear reaction where light nuclei associate to form heavier nuclei. Usually other subatomic particles and energy are part of this reaction, either as reactants or products, as shown in the scheme of a typical nuclear fusion reaction in Figure 2.1. In nature, fusion nuclear reactions power stars like the Sun.
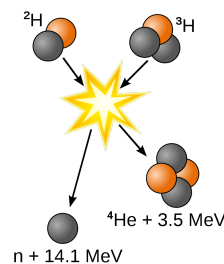


**Figure 2.1**  Fusion of deuterium with tritium creating helium-4, freeing a neutron, and releasing 17.59 MeV [6].

For this process to take place, atoms, who have been stripped of their electrons due to being in plasma state and thus, now, positively charged, must get extremely close together. However, the closer they get, the greater it is the electrostatic repulsion force between the protons of the different nuclei. The final state would never be stable if no other force, that counteracted the repulsive one, existed. That force is the strong nuclear force, which tries to keep nucleons, placed at distances between 1 fm and 0.7 fm, together.

The strong nuclear force, being a very short-range force, cannot offset the electrostatic force at greater distances and that is the reason why fusion reactions are not spontaneous. Therefore, a certain amount of

energy, known as Coulomb barrier, must be given so different nuclei overcome the repulsive electrostatic force and get in the range of action of the strong nuclear force.

That energy explains why, as stated before, matter is in plasma state. However, energy is not the only key for a sustained fusion reaction. A massive pressure is also required to keep nuclei confined so there is enough density of matter for nuclei to collide and not escape. That condition exists, indeed, in the core of the Sun and other stars, thanks to their hugely strong gravity.

Although this process can be endothermic or exothermic, only the latter is desired for the purposes of energy generation since it releases more energy than it needs to happen. The nature of each reaction can be justified using the concept of nuclear binding energy. The nuclear binding energy is defined as the energy required to bring all nucleons (neutrons and protons) from a nucleus apart. In Figure 2.2, the average nuclear binding energy per nucleon for the most common atoms is represented.
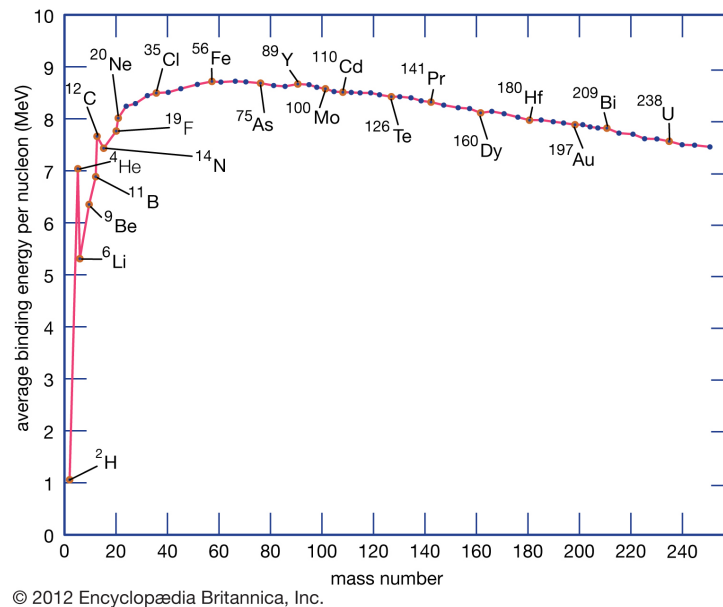
**Figure 2.2** Average nuclear binding energy per nucleon [7].

The most tightly bound nucleus are nickel-62, iron-58 and iron-56. In fact, this last element is represented near to the peak of the curve. That means it is one of the most stable elements existing in nature.
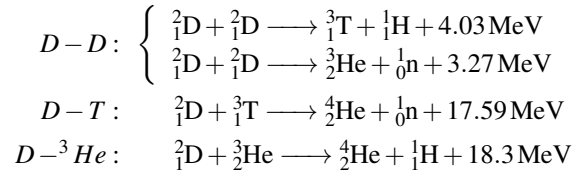
From this perspective, fusing light nuclei (lighter than nickel-62) to form a heavier nucleus results in an increase of the nuclear binding energy and therefore, energy is released. This is what has been called a fusion reaction. On the opposite side, the fission reaction implies the division of heavy nucleus (heavier than nickel-62) into lighter nuclei which also results in an increase of the nuclear binding energy and obviously, energy is released again.

From the figure, it can also be extracted that a fusion reaction releases far more energy than a fission reaction since the slope of the curve is much higher for the light nuclei than for the heavy nuclei, and hence a nuclear reaction for light nuclei implies a bigger change in the nuclear binding energy.

Energy released in these reactions are due to the difference of masses between reactants and products, known as mass defect, as Einstein's famous formula states:

$$E = mc^2$$

Many fusion reactions would theoretically meet those requirements but only a few ones are viable from a technological and efficiency point of view. Thus, we can, for instance, fuse two deuterium nuclei $(D-D)$, one deuterium and one tritium nuclei $(D-T)$ or one deuterium and one helium-3 nuclei $(D-^3He)$.

$$D-D: \begin{cases} {}_1^2D + {}_1^2D \longrightarrow {}_1^3T + {}_1^1H + 4.03\,\text{MeV} \\ {}_1^2D + {}_1^2D \longrightarrow {}_2^3He + {}_0^1n + 3.27\,\text{MeV} \end{cases}$$

$$D-T: \quad {}_1^2D + {}_1^3T \longrightarrow {}_2^4He + {}_0^1n + 17.59\,\text{MeV}$$

$$D-^3He: \quad {}_1^2D + {}_2^3He \longrightarrow {}_2^4He + {}_1^1H + 18.3\,\text{MeV}$$

Among the different candidates, one rises above the others in terms of efficiency, that is the D-T fusion reaction. The vertical axis of the Figure 2.3 represents the fusion cross section, the higher the cross-section, the most probable the fusion reaction is, and the horizontal axis represents the kinetic energy of the reactants, which can be directly translated to temperature. In view of said figure, the D-T fusion reaction reaches its peak of probability at a much lower temperature than other reactions and the cross section at that temperature is higher than any other at any temperature. In addition to that, a single D-T reaction produces 17.59 MeV of energy, more than most other fusion reactions.
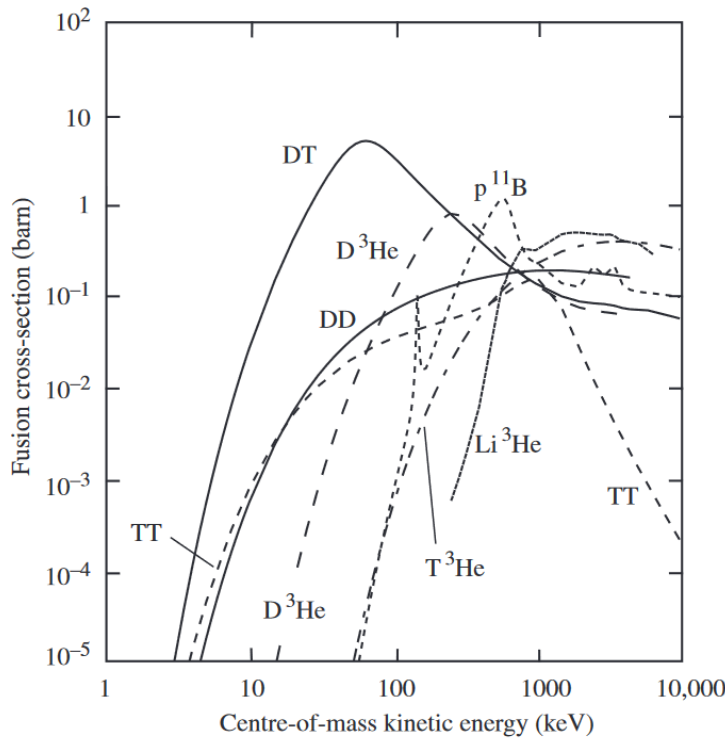


**Figure 2.3**  Fusion cross sections for different reactions [8].

In light of the superior characteristics of the D-T reaction that have just been presented, there is no doubt why most important fusion projects are based on this reaction. However, not everything in this reaction is wonderful. The D-T reaction requires deuterium and tritium in an approximate 50-50 proportion and, while deuterium is incredibly common on Earth (1 liter of seawater contains 33 miligrams of deuterium), tritium is almost non-existent. Tritium must, therefore, be produced artificially, usually from a process that requires lithium which is far more common than tritium. This low natural existence ratio of tritium can be partially explained by another of the D-T fusion reaction particularities: tritium is radioactive and naturally decays into helium-3 by beta decay, although this radioactivity is quite harmless since tritium half-life is about 12-13

years and its radiation can penetrate only about 6.0 mm of air. One last particular aspect is that D-T reactions eject high energy neutrons that due to its neutrality go through everything they encounter, eventually inducing radioactivity in the surrounding materials.

For some projects, specially for those with an important research purpose or those which are planned to be upgraded several times through their life, the neutron activation and radioactivity of the tritium of the D-T reaction that have just been described might not be acceptable because of the big decommissioning issues that this carries. Instead, the D-D reaction is usually preferred in those cases, since those issues are far more limited [9]: the neutrons that are produced in D-D reactions carry less energy and the their irradiation damage is two orders of magnitude smaller when compared to the D-T reactions; tritium is only produced in one of the two D-D possible reactions meaning that its impact is minimized with respect to the D-T reactions. This is the case, for example, for the JT-60SA tokamak, which this work is based on, that has been designed to perform D-D fusion reactions.

## 2.2   Tokamaks

Since 1938, when the first attempt to build a working fusion reactor was made [10], there have been a handful of fusion reactors proposals. As it was already explained in section 2.1, in order to achieve a sustained fusion reaction, it is essential to heat and to confine the plasma.

Regarding the heating of the plasma, stars obtain this energy mainly from their own fusion reactions and so is the idea for the terrestrial fusion reactions. However, while stars are always burning, some way to start and support this process is needed on Earth. With respect to the confinement of the plasma, stars have it quite easy since their gravity is capable of keeping plasma matter together but, on Earth, such gravity does not exist. In general, there are two main approaches for solving these issues:

- The first one is the magnetic confinement fusion (MCF) [11]. As it will later be expanded in sub-section 2.2.1, the matter that will be fused is heated thanks to different mechanisms until it reaches temperatures of hundreds of millions of celsius degrees, becoming hotter than the core of the Sun, and turning into plasma. In this state, nothing is able to physically contain the plasma; any surface touching the plasma would result damaged and, what is worse, the plasma would immediately cool down and the fusion reactions would stop. The technique that this approach uses is to keep the plasma inside a high vacuum vessel, relatively far from the walls, thanks to the use of powerful magnets. The complex magnetic fields that are created serve to control and stabilize the plasma, supporting the fusion reactions performance.

- The second approach is the inertial confinement fusion (ICF) [11]. In this approach, lasers are used in order to heat and compress small pellets of fuel, which can be in solid or gas state. Then, these pellets reach temperatures of fusion and an instant later they blow apart. It is during the nanoseconds between these two moments that fusion power is produced.

Tokamaks are a type of reactor based in the first approach, but they are not alone in this category, another type of magnetic confinement fusion reactors are stellarators. Even so, tokamaks have received the most research and development of all existing fusion reactor proposals and their state of the art is the most advanced one.

Tokamaks were first devised by U.S.S.R. scientists back in 1950. It is a Russian acronym for "toroidal chamber with magnetic coils". Effectively, tokamaks have the shape of a torus and use powerful coils to confine plasma in its interior.

Since then, tokamaks have already proved their effectiveness and reliability and have been built all around the world: JET (United Kingdom), JT-60SA (Japan), ASDEX Upgrade (Germany) or ITER (France) are just some examples of important tokamaks whose impact in the field will be later expanded in subsection 2.2.2. In any case, further research is being carried out thanks to these tokamaks towards the final goal of achieving a burning plasma, where the energy produced is larger than the energy needed for the reaction to take place, and, eventually, having a competitive form of power generation.

### 2.2.1 Structure of a Tokamak

Tokamaks are complex assemblies where pieces coming from almost every field of science and engineering are met. In the Figure 2.4 the main inner components of a modern tokamak can be seen. Slight variations can occur depending on several factors like the type of reaction that will take place inside the reactor or the heating systems considered. Next, some of these components will be detailed.
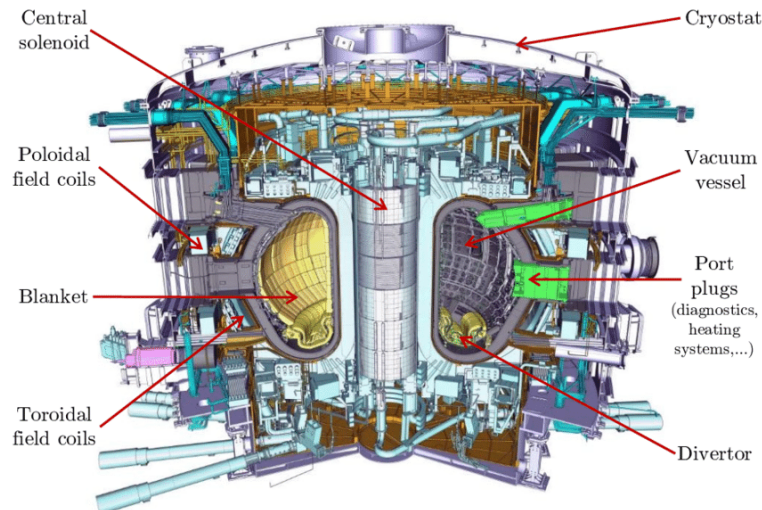


**Figure 2.4** Main inner components of the ITER tokamak [12].

#### Vacuum vessel

The vacuum vessel is a torus shaped hermetical container inside which the plasma is confined. It is sealed in a way to preserve a high-vacuum environment while allowing some systems to pass through it such as the heating systems or the diagnostics and several apertures for maintenance.

Contrary to what could be expected, instead of mimicking the high pressure existing in the stars, it is preferred a high-vacuum environment for the plasma. To replace that high pressure which is needed to hold the plasma together, scientists have figured out how to use magnetic fields to do the same task. One of the main reasons for the necessity of this low pressure is that many atoms in the atmosphere would contaminate the plasma and make it unsustainable otherwise.

The vacuum vessel also acts as a first safety containment barrier against radiation and radioactivity. Additionally, it has a structural function since it holds other pieces such as the blanket or the divertor.

#### Blanket

The blanket covers the inner walls of the vacuum vessel and it is exposed directly to the plasma, protecting other components from the enormous temperature of the plasma and the high energy neutrons that are ejected in some fusion reactions.

There are many variants of blanket configuration but the most typical parts existing in the blanket are the heat resistant tiles, which can be made of graphite or beryllium, and the nuclear shield blocks which provide protection against powerful neutrons produced during some fusion reactions. Additionally, an active cooling system is responsible for the extraction of heat, which is expected to eventually serve for energy generation purposes.

### Divertor

Known as the "ashtray" of tokamaks, the divertor must face enormous heat loads. The divertor allows the removal of any undesired particle that enters the vessel as well as other heavy ions resulting from fusion reactions that would act as impurities and affect negatively to the proper operation of the tokamak.

### Magnet system

One of the main obstacles in nuclear fusion is the confinement of the plasma and the control of plasma instabilities. Thanks to the ionized nature of the plasma, a complex magnet system consisting on a generous amount of powerful superconducting coils and other passive components, is the adopted solution for this issue in tokamaks.

Thanks to the superconductivity property, magnets are able to carry a higher current and hence produce a stronger magnetic field. Nowadays, the main way to achieve superconductivity is at a very low temperature and that is why those magnets must be internally cooled.

### Cryostat

The cryostat houses the previous components and, similar to the vacuum vessel, it must protect the high-vacuum environment that has to exist in the interior of the tokamak. Moreover, the cryostat provides the ultra-cool environment necessary to insulate some temperature-critical components.

### Heating system

In order for matter to be in plasma state, it has to reach a temperature of million of degrees. For this purpose, several heating mechanisms can occur (usually simultaneously) in a tokamak:

- **Ohmic heating**: The magnets, which are used to control the plasma, induce a high-intensity current in the core of the plasma. According to the Joule effect, and since the plasma has a certain electrical resistance, some heat is generated. However, this mechanism becomes insignificant when plasma temperatures are too high because of the decrease of plasma electrical resistivity with the temperature.

- **Neutral beam injection (NBI)**: It consists in shooting neutral particles with a very high velocity into the plasma. When the neutral particles collide with plasma particles, energy is transferred in the form of heat.

- **High-frequency electromagnetic waves**: The energy that these electromagnetic waves carry is absorbed by plasma ions or electrons, depending on the frequency of the waves, making them heat up.

- **Burning plasma**: Since fusion reactions in tokamaks are exothermic, it is important that those reactions themselves are able to partially sustain the temperature of the plasma.

From these mechanisms, the second and the third one require external heating systems which must pass through the vacuum vessel in order to face the plasma.

### Diagnostics port

It is crucial to supervise the interior of the tokamak in order to control and study the plasma. This is partially done thanks to many standard devices known as diagnostic port plugs, capable of measuring a wide variety of parameters. They are housed in a drawer-like steel structure known as diagnostics port, that goes through the cryostat and the vacuum vessel.

### 2.2.2 JT-60SA and its context

The path to a controlled nuclear fusion has been long and agitated since its beginning. Nowadays, most of the sights are set on the development of ITER (International Thermonuclear Experimental Reactor), the most powerful tokamak to ever be built until now. ITER is expected to be the first nuclear fusion reactor to achieve the plasma energy breakeven that indicates that the power generated by the reactor is greater that the power needed to produce it. The objective of ITER, apart from proving the technical feasibility of nuclear fusion energy generation is to serve as a major testing ground for nuclear fusion experiments to better understand plasma behaviour and to find potential reactor improvements.

Since ITER is a gigantic project, many so-called satellite projects work together with ITER in order to solve every kind of obstacles ITER may encounter. Here we can find JET (Joint European Torus), which is currently the largest and most advanced tokamak in the world. JET has been reconverted from a project of his own, whose goal was to reach the plasma energy breakeven, to a "test bed for ITER technologies and plasma scenarios" [13]. Another satellite project is the JT-60SA tokamak installed in Japan, which is the one this work is based on. JT-60SA, whose interior is shown in Figure 2.5, has been designed to support ITER but also to study how to optimize the design and operation of future nuclear fusion reactors such as DEMO.
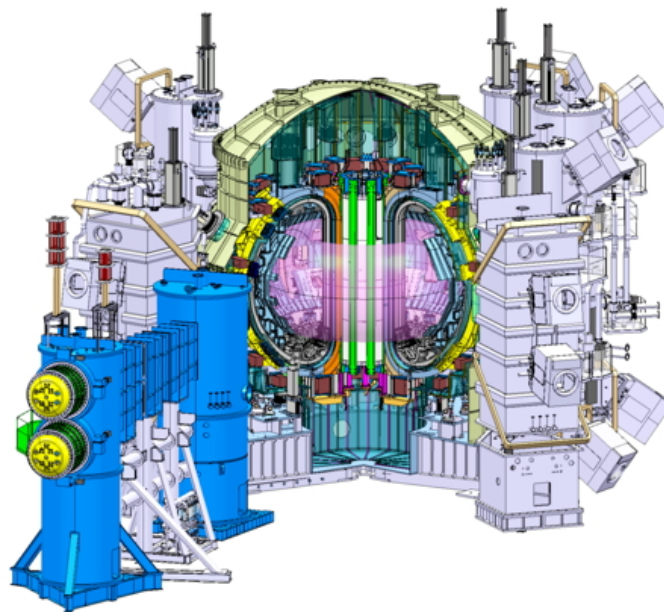


**Figure 2.5** Scheme of the interior of the JT-60SA tokamak [14].

DEMO (DEMOnstration Power Station), which is already being designed, is the next step after proving nuclear fusion technical feasibility. DEMO's mission is to get closer to a commercial nuclear fusion reactor by generating electricity with an even greater gain factor than ITER.

Other reactors like Wendelstein 7-X, which is represented in Figure 2.6, are based on the stellerator design and advances in parallel with the previously mentioned projects. Apart from cooperating in many aspects with them, it could eventually serve as a back-up option if tokamak models encounter a major obstacle impossible to overcome or if stellarator models just end up working better.

### 2.2.3 Fast ions in tokamaks

It is interesting for this work to explain what fast ions are. Fast ions are ions that are usually located at the centre of the plasma. They can have two origins, either generating from the fusion reactions themselves or from the external heating mechanisms. Fast ions differ from other ions and electrons in the plasma in that
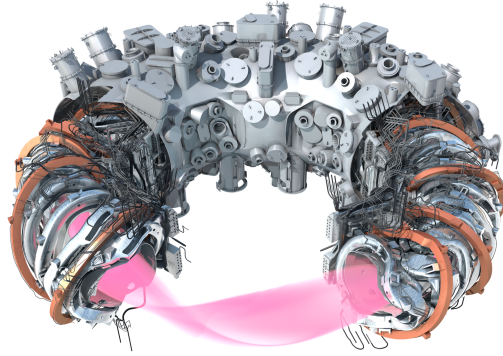
**Figure 2.6**  Rendering of the interior of the Wendelstein 7-X stellarator [15].

they carry a higher energy thus having a higher temperature, and that they are responsible for the continuous heating of the plasma.

It is important to optimize their confinement within the plasma since fusion reactions sustainability and performance greatly depend on it. However, fast ions behaviour is unpredictable to a certain degree and some of them are capable to escape the magnetic confinement. Losing them hinders the proper confinement and amplifies plasma perturbations, and could even damage the tokamak integrity. [16].

With that goal in mind, the characteristics of fast ions must first be studied. One aspect to accomplish it is the measure of fast ion losses which is possible thanks to a diagnostic port plug called fast ion loss detector (FILD). The thermal analysis of the FILD being designed for the JT-60SA tokamak is the subject of this work.

**Fast ion loss detector (FILD)**

Fast ion loss detectors are based on the behaviour of scintillator materials. When those materials are impacted by particles, they emit a light signal in the position of the impact.

As shown in Figure 2.7, a scintillator plate is housed inside a cap which is made of graphite due to its great thermal properties. In order for fast ions to reach that scintillator plate, they have to pass through a pinhole and a collimator. This mechanism filters the fast ions that are going to be measured which helps narrowing the range of possible candidates. Then, thanks to the existing magnetic field and depending on the characteristics of these ions, the position of impact against the scintillator plate determines the ions pitch angle and gyroradius.
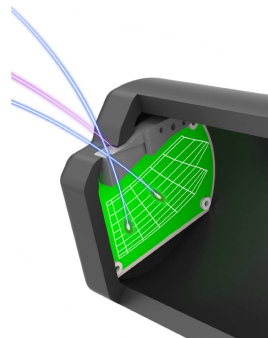


**Figure 2.7**  Representation of fast ion detection in FILD [17].

When the impact happens, a light signal is produced and thanks to a series of lens and optic devices, this signal is then redirected to a couple of cameras. One of them is the responsible for registering the position of the impact with a very high precision. The other one captures the rate of impact of those ions. With that information, scientists are capable of analysing some characteristics of the fast ions that escape the confinement.

In order to perform these measurements, FILD must approach the plasma, approximately to the level of the vacuum vessel. In that position, the heat fluxes are very high and it is very difficult to operate. For this reason and to guarantee the detector integrity, a retractile mechanism is used to back off FILD while not measuring so it can cool down.

# 3  Motivation, objectives and methodology

In this chapter, the motivation of this work and the main milestones taken in consideration in order to achieve our goals will be presented.

## 3.1  Motivation of the work: The JT-60SA FILD

The JT-60SA FILD, whose thermal assessment is at the core of this work, will be installed within a port plug in the equatorial diagnostic port and held by the main diagnostics flange.

The mechanical design of the FILD components, which is shown in Figure 3.1, allows the probe head, that houses the scintillator, to move between the parking position and the measuring position. The mission of the mechanism is to provide about 1 meter of linear displacement for the probe head.
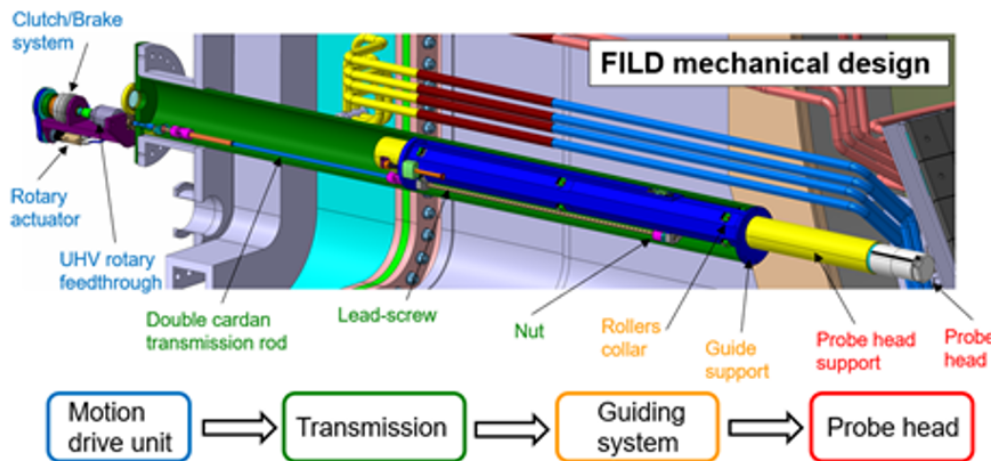


**Figure 3.1**  JT-60SA FILD mechanical design: the motion of the probe head is provided, ex-vessel, by the drive unit, transferred to the head support by a lead-gear and guided by roller collars attached to the fixed guide support [18].

To obtain the linear stroke of the probe head, a reversible pneumatic rotatory motor initially provides some torque. This torque, which must be limited by a pneumatic clutch because of constructive reasons, is then transmitted to the interior of the vacuum vessel by means of a pulley-transmission belt system and a bellow-based rotatory feedthrough while keeping intact the high vacuum inside the vacuum vessel. The rotation is then transferred from the feedthrough to a lead gear system by means of a double universal joint that cancels

any possible axial misalignments that might exist between components so far apart. Finally, the lead gear transforms the rotatory displacement into a linear one. The resulting displacement is guided by roller collars which also help to decrease the friction between fixed and moving parts.

As it was mentioned in the previous chapter, FILD is subjected to very high heat loads, specially in the measuring position. Although FILD materials are capable of handling high temperatures, they must be checked to avoid any undesirable surprise. For instance, stainless steel temperature of recrystallization is above 1000 ºC, graphite sublimates at more than 2000 ºC and the scintillator material becomes permanently inoperative when it reaches 500 ºC.

Moreover, the measurements could not be optimal at high temperatures. It is specially important in the case of the scintillator plate. When the scintillator plate exceeds temperatures of about 200 ºC, the light signals derived from the impact of ions start becoming more and more difficult to be analysed since the scintillator plate itself emits light due to its own temperature.

The aim of this work is to determine the design and operating mode of FILD so the components are kept in an acceptable range of temperatures according to their material properties and to their performance requirements.

## 3.2  Objectives and methodology

First of all, the temperature of the components of FILD must be tracked at every moment of the tokamak operation. For this, several thermal simulations are going to be executed using an appropriate software. In this case, the chosen software for these simulations will be Ansys Workbench.

In order to run these simulations it is necessary to create a thermal model and apply different boundary conditions such as thermal loads and temperatures to some of its elements. This will mainly be done in the same software, Ansys Workbench, although other software programs, such as MATLAB or CATIA, might be of help for certain actions.

Some optimizations will be performed to determine the best choices for some questions that may be encountered. Once the exact equations involved in these optimizations are identified, it is rather straightforward to perform the optimizations in a numerical computing software such as MATLAB. However, for more complex optimizations, it has also been studied how to implement them in Ansys Workbench.

Finally, in order to illustrate and analyse the results given by the simulations and optimizations, they will be represented in graphics using Ansys Workbench and MATLAB capabilities as can be seen in Figure 3.2.
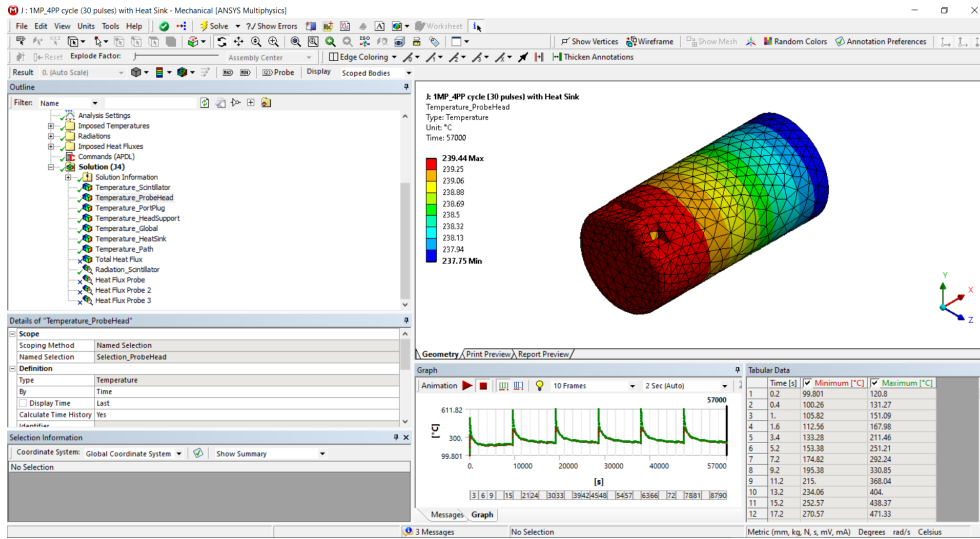
**(a)** Ansys Workbench workspace.
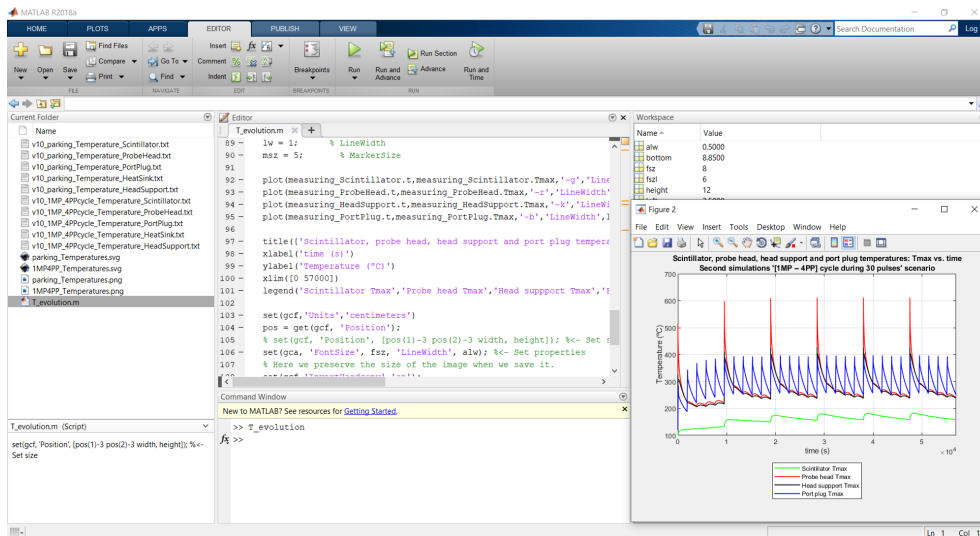


**(b)** MATLAB workspace.

**Figure 3.2** Aspect of the workspace of the software used in this work.

# 4 Preliminary thermal assessment

In this chapter, a preliminary thermal model for FILD will be constructed. Then, a finite element analysis will be performed using that model. Finally, the results from that analysis will be shown and evaluated in order to conclude if the temperatures of the components are satisfactory according to the objectives defined in chapter 3.

## 4.1 Thermal model

In this section, the following details of the thermal model that will be constructed for the finite element analysis are presented: a description of each component of the model, the decisions that will be made about their geometry and the geometry itself; the materials that will be used for each component and the thermal properties of those materials; the boundary conditions that will be applied, in particular, the temperatures that will be imposed to some surfaces and the heat fluxes that will exist; the operation modes of FILD that will be designed, deciding the intervals of time when the probe head shall be in measuring position or in parking position; and some small adjustments before launching the simulations.

### 4.1.1 Geometry

The general geometry of the model is shown in Figure 4.1. This is a simplified geometry of the real one, already presented in Figure 3.1, since it would take an enormous amount of time to perform the simulations otherwise; not all the parts are included and those which are, have a simpler geometry compared to the real ones. However, the most relevant parts for the thermal analysis have been added and those that while being relevant have not been included, have been replaced by thermal conditions. Next, each part of the geometry of the thermal model is being detailed.
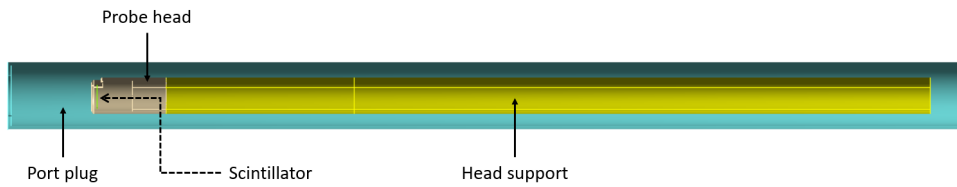
#### Diagnostics port

The diagnostics port is a structure made of structural steel that houses the diagnostic port plugs. In this case, only FILD has been modelled but it cannot be forgotten that it is surrounded by a handful of other diagnostic port plugs like the one used to install FILD.

In order to model the geometry of the diagnostics port, the real model has been exported from CATIA and imported to Ansys Workbench. There, the inner surfaces have been extracted and, since this part is going to be used to simulate the thermal environment for FILD, it has been modified to create a closed surface.
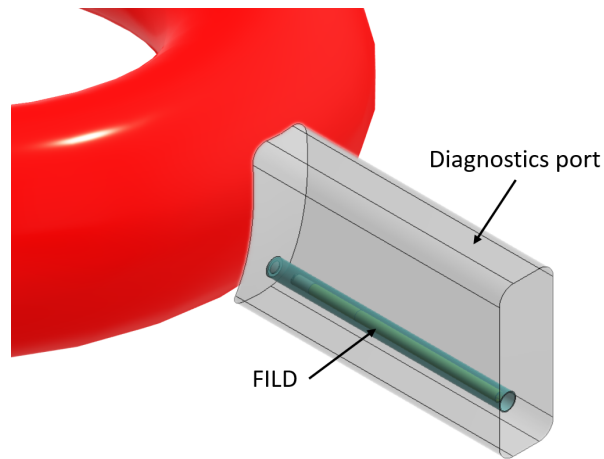
**(a)** A global view of the geometry of the model. A coarse illustration of the plasma has been represented (red toroid) for the purpose of clarification but it is not part of the model.



**(b)** A more in detail view of the interior of FILD model in parking position.

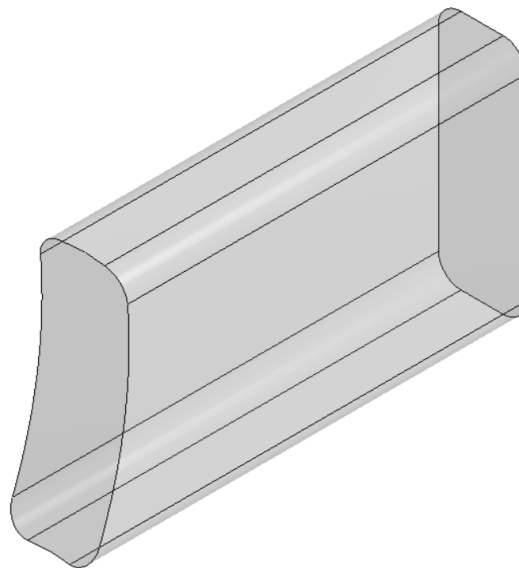**Figure 4.1**  General geometry of the thermal model.



**Figure 4.2**  Diagnostics port model geometry.

### Port plug

The port plug geometry has been fully modelled in Ansys Workbench. It is made of structural steel and serves as a structure and thermal protection for the internal components of FILD.

FILD port plug is a standard part, with dimensions similar to the other port plugs, and it is connected in his back to the diagnostics port by a flange that has not been modelled, giving place to a boundary condition that will be later described.

In the port plug plasma facing face, it has an aperture that allows the probe head to pass through it, with a very small gap, in order to hide from plasma and receive lower heat fluxes or approach the plasma and start measuring.
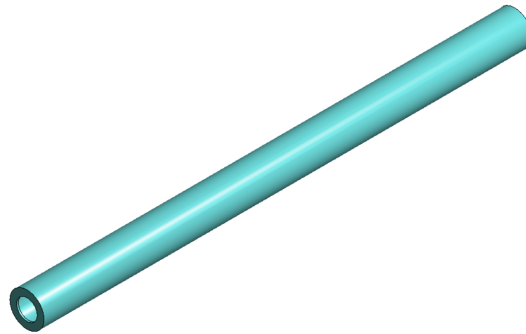


**Figure 4.3**  Port plug model geometry.

### Probe head

The probe head is the most exposed part to plasma of all FILD components. Hence, it is made of graphite due to the great thermal properties of this material like its very high melting point.

The geometry of the probe head plays an important role in the measurement of fast ions and was therefore already designed based on physics simulations developed to maximize the measured signal. Its 3d model has been directly exported from CATIA and imported to Ansys Workbench.
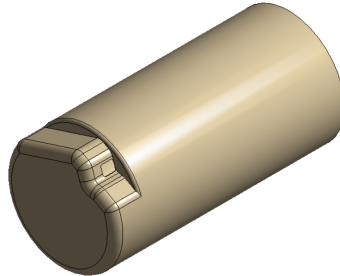


**Figure 4.4**  Probe head model geometry.

### Scintillator

In the interior of the probe head, it is housed the scintillator. The scintillator, which was already designed, has been remodelled in Ansys Workbench with a simpler geometry for the purpose of this study. The face where ions will impact, has been positioned at the level of the probe head collimator and a thin width has been applied to it. The connection to hold the scintillator plate to the probe head has not been modelled. However, it is known that it is a low thermal conductivity connection (otherwise an important heat flux from the probe head would reach the scintillator) and therefore a new thermal condition that insulates it from the heat transfer by conduction will be created.

### Head support

The head support, as its name suggests, serves as support for the probe head. It is a component of the retractile mechanism that allows the movement of the probe head from the measuring position to the parking position

**Figure 4.5**  Scintillator model geometry.

and vice versa. Another objective of the head support is to cool down the probe head via radiation to the cooler parts of the port plug thanks to its large external surface area.

The rest of the retractile mechanism, consisting on a lead screw, linear motion guides and a double cardan joint among other structural components, has not been modelled due to its complexity. An unknown amount of heat that would flow through these components by conduction has not been included since their contact surfaces are very small making this heat transfer mechanism negligible.

The head support has been modelled in Ansys Workbench as a hollow tube made of structural steel, with the same section as the probe head in its connection surface, and a generous length that improves the previously mentioned heat transfer.
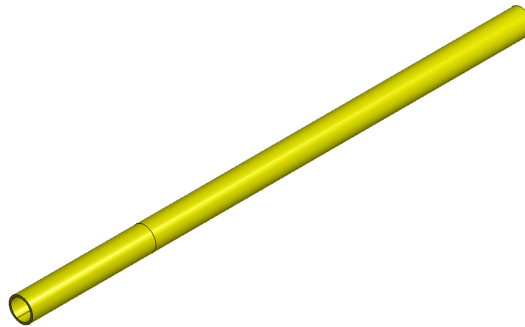
**Figure 4.6**  Head support model geometry.

### Parking position

There are decisions in the geometry modelling that have been taken with a relevant underlying study. This is, for instance, the case of the parking position.

The parking position distance is the distance from the probe head to the tip of the port plug while not measuring (parameter $d$ in Figure 4.7). This distance allows for a better cooling of the probe head at the cost of a longer mechanical stroke and deploy times.

To determine this distance the equation (4.1) [19] has been used. This equation stipulates the amount of radiative heat flux that arrives to a surface retracted by a distance inside a clearance hole, which is equivalent to the aperture found on the port plug of FILD. The parameters of this equation, which are represented also represented in Figure 4.7, are:

$P$, which is the radiative heat flux arriving to the retracted surface of the probe head

$P_0$, which is the radiative heat flux at the tip of the port plug

$d$, which is the retraction distance

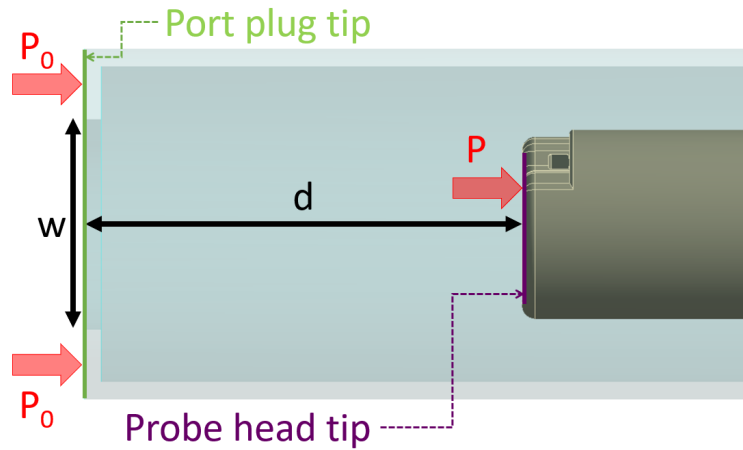$w$, which is the diameter of the aperture of the port plug

**Figure 4.7** Parking position parameters.

$$P = \frac{\left(\frac{w}{2}\right)^2}{d^2 + \left(\frac{w}{2}\right)^2} \cdot P_0 \tag{4.1}$$

This equation includes parameters, other than the retraction distance, that must first be resolved:

- In particular, the heat flux arriving to the surface of the tip of the port plug depends on its distance to the plasma. Its value ($P_0 = 0.03764 W/mm^2$) will be later determined in subsection 4.1.3 considering that it is placed at the same distance as other already existing port plugs. There might be some discussion about the choice of this parameter; however, it has been found that for a same mechanical stroke of the probe head, a variation in the position of the port plug is not very relevant from a thermal point of view.

- For the diameter of the aperture of the port plug, the size of the probe head has been taken into consideration, leaving a small gap between both of them when the probe head is passing through the port plug aperture as can be seen in Figure 4.8.
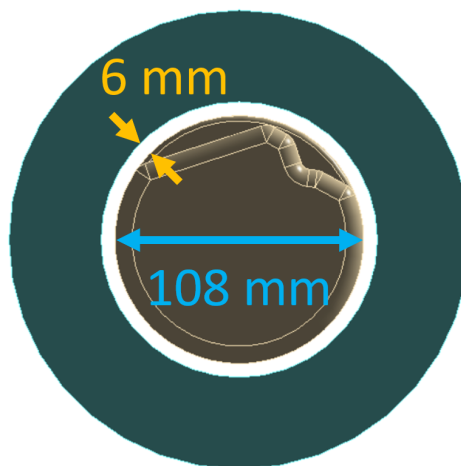


**Figure 4.8** Gap between the probe head and the aperture of the port plug.

Now, with these parameter values, the resulting heat flux from the plasma at the surface of the probe head with respect to the parking position distance has been plotted in Figure 4.9.
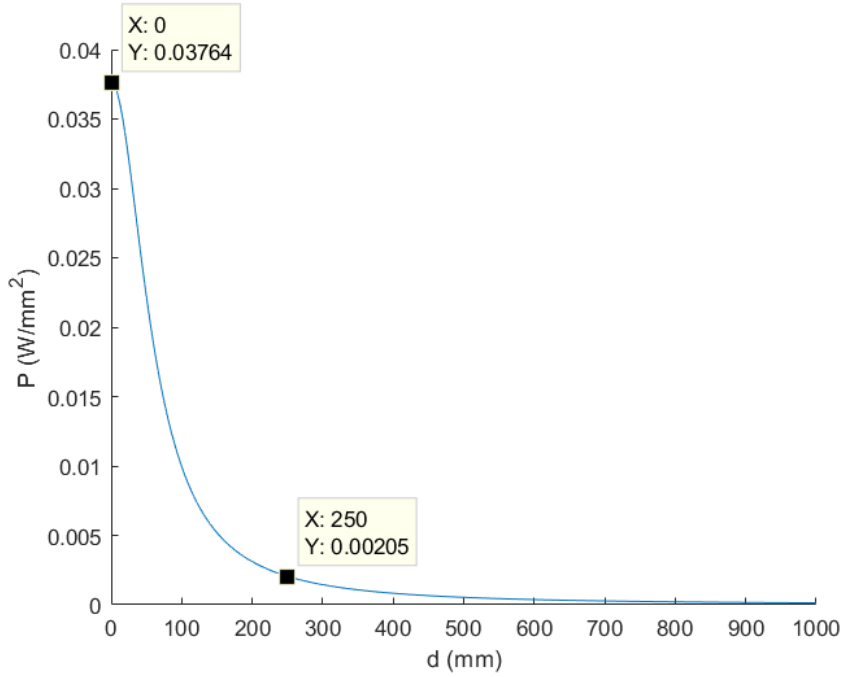
**Figure 4.9** Heat flux received by the probe head in parking position vs Parking position distance.

It was already expected that the heat flux that the probe head would receive from plasma when in parking position would decrease the deeper it was inside the port plug. However, it is not known yet where the parking position should be established but it can be observed that there is a great slope at the beginning of the curve that becomes very small at long parking position distances. This means that the profit gained from increasing the parking position distance when those distances are small is greater than when those distances are long. This behaviour can be better observed by deriving the equation (4.1) with respect to the parking distance.

$$\frac{dP}{dd} = -2P_0 \cdot \left(\frac{w}{2}\right)^2 \cdot \frac{d}{\left(d^2 + \left(\frac{w}{2}\right)^2\right)^2} \tag{4.2}$$

The new equation, (4.2), has been plotted in Figure 4.10 and it can be seen that it has a minimum where the profit of increasing the parking position distance is maximum. That minimum can be obtained by deriving again the (4.2) and setting it equal to zero. The minimum is located at $d^* = \sqrt{\frac{w^2}{12}}$ independently of the value of $P_0$, and takes a value of $\frac{dP}{dd}(d^*) = -2P_0 \cdot \left(\frac{w}{2}\right)^2 \cdot \frac{3\sqrt{3}}{16}$.

Now that the location and the value of that minimum is known, the decision of where the parking position is going to be established must be made. A discussion over this aspect could eventually arise again, but taking into account the disadvantages of increasing the parking position distance previously mentioned at the beginning of this section, it has been decided that a distance where the profit of increasing the distance is about a 5% of the maximum previously found would probably be a reasonable choice.

In order to visualize this concept more clearly, the equation (4.2) has been divided by its minimum value located at $d^*$, and the resulting equation (4.3), which is also independent of $P_0$, has been represented in Figure 4.11.
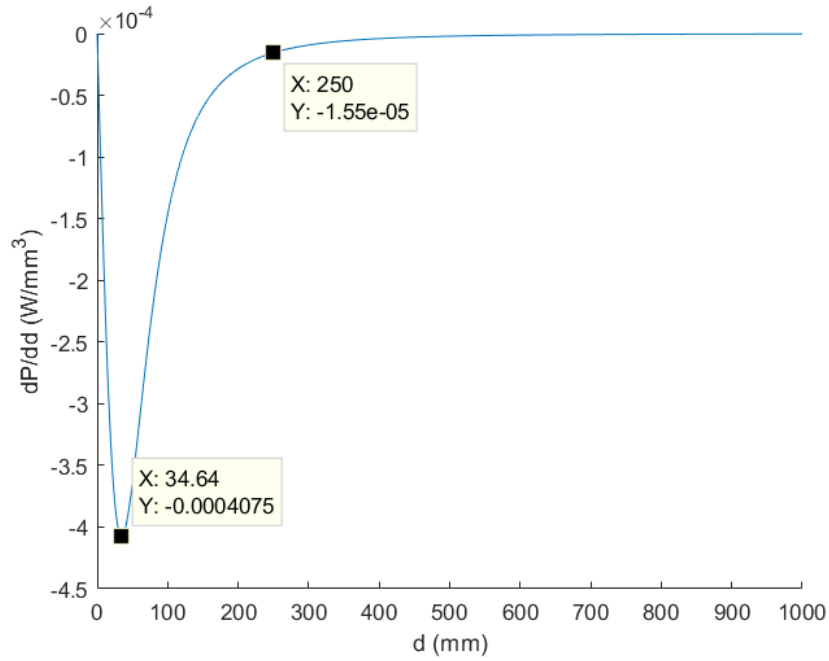
**Figure 4.10**  Derivative of the heat flux received by the probe head in parking position with respect to the parking position distance vs Parking position distance.

$$
\left.\frac{dP}{dd}\right)_{rel} = \frac{\frac{dP}{dd}}{\frac{dP}{dd}(d^*)} = \frac{16}{3\sqrt{3}} \cdot \left(\frac{w}{2}\right)^3 \cdot \frac{d}{\left[d^2 + \left(\frac{w}{2}\right)^2\right]^2} \tag{4.3}
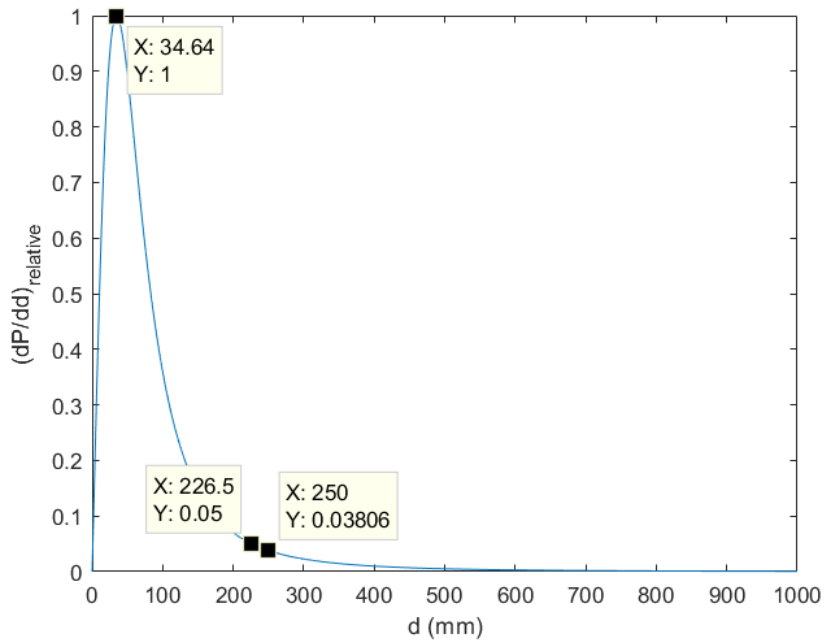$$



**Figure 4.11**  Relative heat flux reduction profit vs Parking position distance.

It can extracted from Figure 4.11 that the distance that was being searched is 226.5 mm, no matter the amount of heat flux arriving to the port plug tip. We are emphasizing in this aspect because, as it has already been commented, $P_0$ only depends on the distance of the port plug tip to the plasma and the port plug could someday be decided to be shortened if it was needed to and, yet, this brief study of the parking position distance would still remain valid.

It has finally been decided to extend this distance to 250 mm, giving a bit of extra cooling for the probe head while not compromising excessively the mechanical behaviour.

### 4.1.2   Material properties

The materials of the components for the first simulations are structural steel and graphite. These materials are already integrated by default in Ansys Workbench but custom materials have been created instead. They mainly differ in that their densities, thermal conductivities and specific heats are now temperature dependent.

The following components have been modelled as made of structural steel with the properties shown in Table 4.1:

- Diagnostics port

- Port plug

- Head support

- Scintillator (although made of a different material, TG-Green, similar properties to structural steel have been supposed)

**Table 4.1**  Structural steel properties.

| Structural steel [20] | | | | | | | | |
|---|---|---|---|---|---|---|---|---|
| Temperature (ºC) | 100 | 200 | 400 | 600 | 800 | 1000 | 1200 | 1500 |
| Density (kg/m$^3$) | 7900 | | | | | | | |
| Thermal conductivity (W/mºC) | 9.2 | 12.6 | 16.6 | 19.8 | 22.6 | 25.4 | 28.0 | 31.7 |
| Specific heat (J/kgºC) | 272 | 402 | 515 | 557 | 582 | 611 | 640 | 682 |
| Emissivity | 0.3 | | | | | | | |

The other material, graphite, whose properties are shown in Table 4.2, has only been used for the probe head.

**Table 4.2**  Graphite properties.

| Graphite [a] | | | |
|---|---|---|---|
| Temperature (ºC) | 0 | 500 | 1000 |
| Density (kg/m$^3$) | 2250 | | |
| Thermal conductivity (W/mºC) | 115 | 63 | 49 |
| Specific heat (J/kgºC) | 638.9 | 1302.3 | 1451.9 |
| Emissivity | 0.7 | | |

[a] Graphite properties have been extracted from ASDEX Upgrade materials library

As it will be detailed in subsection 4.1.3, the emissivity values have only been applied to certain surfaces of the components.

### 4.1.3 Boundary conditions

**Temperatures imposed**

Two surfaces have seen their temperature fixed, either as a constant or as a distribution:

- The rear surface of the port plug, where it is supposed to be connected by a flange to the diagnostics port, has been imposed a fixed temperature of 25 ºC as shown in Figure 4.12.

- A temperature gradient has been imposed to the diagnostics port, with a maximum of 100 ºC near the plasma and a linear decrease with the distance up to a minimum of 25 ºC at the farthest point from the plasma, as can be observed in Figure 4.13. This is an estimate of the temperature of the environment surrounding FILD at a representative moment of the tokamak operation.
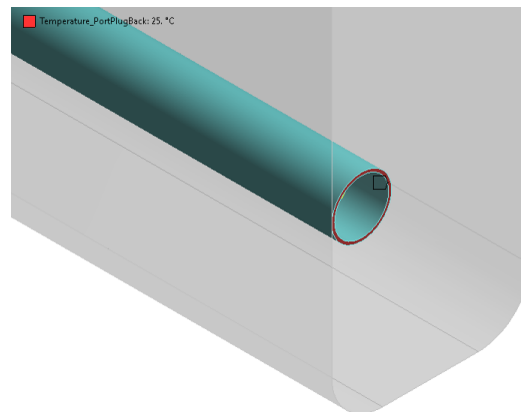


**Figure 4.12**  Fixed temperature of 25 ºC at the flange surface of the port plug.
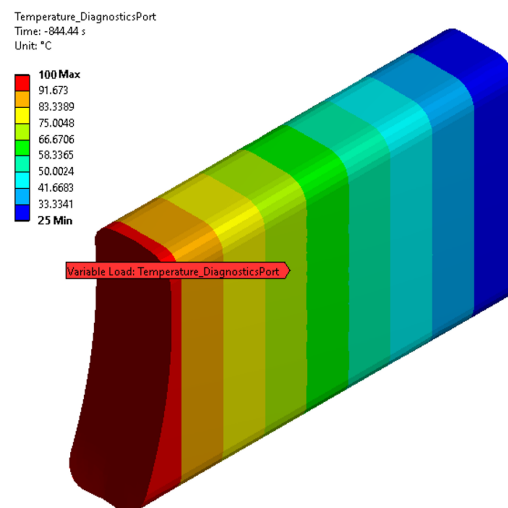


**Figure 4.13**  Diagnostics port temperature gradient ranging from 100 ºC to 25 ºC.

**Simulated heat fluxes**

Under this category have been grouped the heat fluxes that naturally occur via conduction, convection and radiation due to a difference of temperature and that are calculated by the simulation software Ansys Workbench.

The whole system is in an ultra high-vacuum environment of about $10^{-6}$ Pa and, hence, there is no possible convection.

Apart from the internal conduction within each component, conduction between different bodies only occurs between the probe head and the head support since they are the only components that have been modelled with a physical connection. A perfect contact has been added between them, since a special ceramic, commercially known as shapal, with high thermal conductivity (and high electric resistance), will be used for the connection. As it has already been said in previous sections, the physical connection between the head support and the port plug has been omitted and, therefore, no conduction will appear between them.

At last, radiation happens between the surfaces that have been given a certain value of emissivity. These surfaces are:

- The internal surfaces of the diagnostics port i.e., the ones that can be seen by FILD.

- All the surfaces of the port plug with the exception of the one where a temperature of 25 ºC has been imposed.

- All the surfaces of the probe head with the exception of the surface where the probe head and the head support make contact.

- Only the surface of the scintillator where ions will impact, since the others are supposed to be covered by a ceramic material with a very low thermal conductivity.

- All the surfaces of the head support with the exception of the surface where the probe head and the head support make contact.

**Imposed heat fluxes**

The reason of being of these other type of heat fluxes is that the plasma cannot be easily modelled. Instead, the heat fluxes that should be arriving to each component due to the plasma radiation and the subatomic particles heat generation have directly been imposed. It is interesting to note that these heat fluxes do not vary with the emissivity of each material since they are fully absorbed by any material due the special characteristics of the wavelength of the plasma radiation.

First of all, it has to be mentioned that tokamaks operate by pulses. In the case of JT-60SA, these pulses work in a cyclical form where during 100 s the plasma is active, with all that this entails, and the next 1800 s there is no plasma. This operation cycle is shown in Figure 4.14.
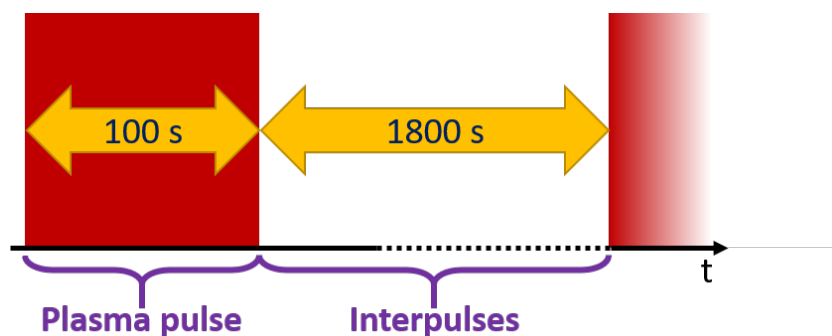


**Figure 4.14**  Scheme of the plasma pulse cycle.

At this point, two positions of FILD must be differentiated: the parking position and the measuring position. These two positions, with the surfaces where heat fluxes due to the plasma heating must be imposed, are

shown in Figure 4.15. The process of applying those heat fluxes is not always straightforward, as it will be seen later, and a combined use of Ansys Workbench and MATLAB will sometimes be required.
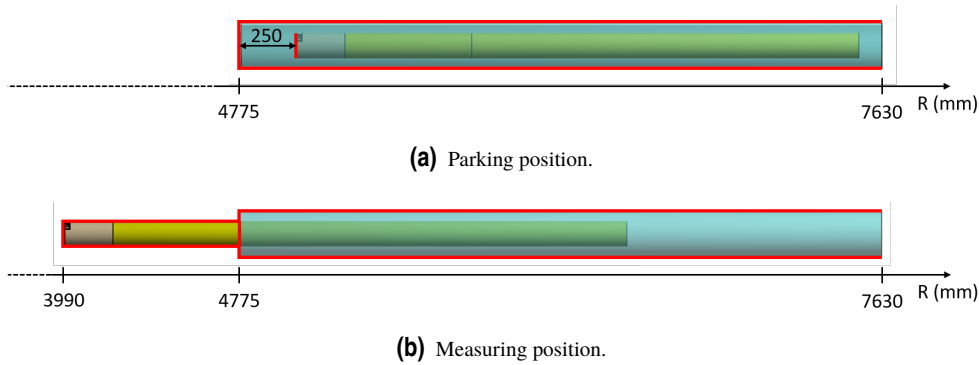


**(a)** Parking position.



**(b)** Measuring position.

**Figure 4.15** General overview of the two positions of FILD and the surfaces that receive heat flux from plasma (red lines) in each case.

In this section a geometrical parameter, $R$, is going to be introduced. It is the radial coordinate of each point with respect to the center of the tokamak seen as a cylinder.

According to the Plant Integration Document (PID) [21], the plasma heat flux arriving at the level of the stabilizing plate, at $R = 3990$ $mm$ (where the probe head tip is placed in its measuring position), is $q = 0.3$ $W/mm^2$ and the evolution of the heat flux with the distance can be approximated by the equation (4.4) [22] which is valid in a range from $R = 4400$ $mm$ to $R = 6200$ $mm$. In theory, this equation is only valid for surfaces that are perpendicular to the plasma; however, it has been used independently of the angle of incidence since it would be very complex otherwise. In any case, the approach taken remains conservative and the reality should turn out to be less aggressive in this aspect.

$$q = aR^4 + bR^3 + cR^2 + dR + e \tag{4.4}$$

where:

$q$ is the heat flux arriving at a surface

$R$ is the previously explained radius for that surface

$a$, $b$, $c$, $d$ and $e$ are parameters with the following values:

$a = 13427.8481934843$ $W/m^6$

$b = -315077.093046085$ $W/m^5$

$c = 2776682.94726302$ $W/m^4$

$d = -10899642.2688492$ $W/m^3$

$e = 16095993.0244847$ $W/m^2$

Since the components of the model are in a range of radius from 3990 mm to 7630 mm, a piecewise-defined function has been created using the data we have. From 4400 mm to 6200 mm, the given equation (4.4) has been directly used. For radius lower than 4400 mm, a linear interpolation between the given heat flux at the stabilizing plate level and the heat flux indicated by the previous equation at 4400 mm has been made. For radius greater than 6200 mm, a heat flux equal to zero has been supposed. This is summarized in the

piecewise equation (4.5), that has been plotted in Figure 4.16 in order to give a better spacial perception.

$$q(R)[W/mm^2] = \begin{cases} 2.369 - 5.185 \cdot 10^{-4} \cdot R & 3990 \ mm \le R < 4400 \ mm \\ aR^4 + bR^3 + cR^2 + dR + e & 4400 \ mm \le R \le 6200 \ mm \\ 0 & 6200 \ mm < R \le 7630 \ mm \end{cases} \tag{4.5}$$
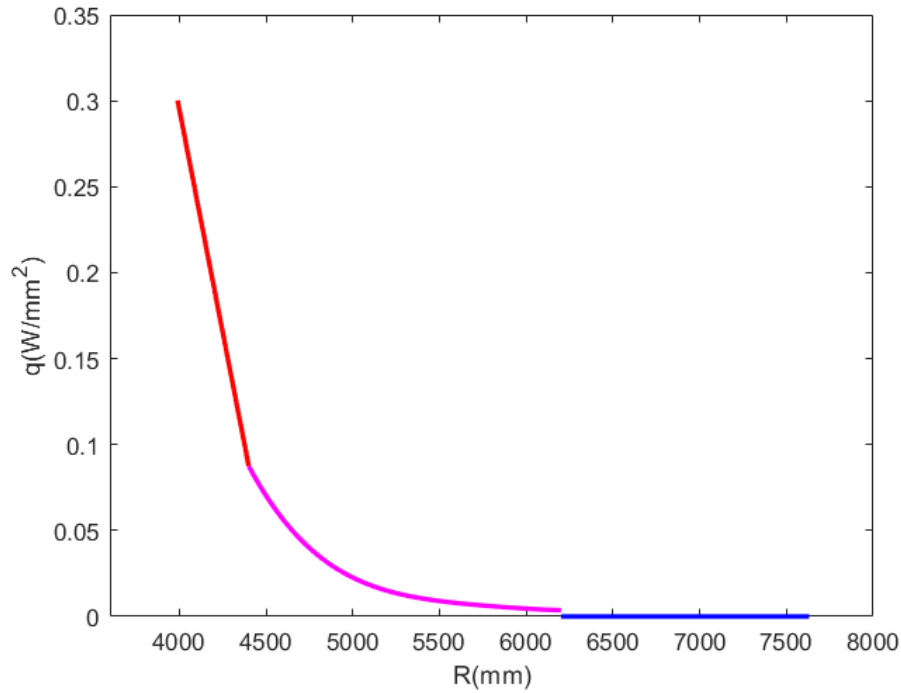


**Figure 4.16**  Plasma heat flux depending on the radius.

In first place, the plasma heat flux at the tip of the port plug is going to be calculated. Apart from being one of the plasma heat fluxes that had to be found, it is needed to calculate the heat flux arriving to the tip of the probe head when it is hiding inside the port plug in parking position. Using the function (4.5) for the radius of the port plug tip ($R_{portplugtip} = 4775 \ mm$):

$$q_{portplugtip} = P_0 = 0.03764 \ W/mm^2$$

Now, introducing this value in the equation (4.1) along with the other parameters previously determined, the heat flux arriving to the tip of the probe head in parking position can finally be obtained:

$$q_{probeheadtip(PP)} = P = 0.00205 \ W/mm^2$$

In second place, the plasma heat flux for the rest of surfaces is going to be calculated. These surfaces are special in the sense that they do not have a constant radius along their area. The approach taken to solve this issue, which is detailed right below, consists on the imposition of heat fluxes at a nodal level combining the use of Ansys Workbench and MATLAB.

**1.** The surfaces of interest have been extracted from the solid bodies of the model.

**2.** Then, following the indications of the ANSYSimport function [23], their model has been exported using APDL commands. From that model, we are only interested in the meshes of the affected surfaces.

**3.** Using again the indications of the ANSYSimport function, the meshes have been imported to MATLAB. Since the meshes of the surfaces created before where composed of triangles, a certain heat flux can now be applied to each one of these triangles knowing their tokamak radius.

**4.** In that same MATLAB program, the meshes with the heat fluxes from plasma that had just been calculated have been exported and written into text files with a format that ANSYS Workbench can interpret.

**5.** Next step, ANSYS Workbench has read those files and imported their content as heat fluxes.

**6.** Finally, each heat flux can now be assigned to the corresponding component surfaces. ANSYS Workbench has, then, interpolated the heat fluxes of the external files to the mesh of the simulation project.

The result of this process can be seen in Figure 4.17 where all the heat fluxes that were meant to be determine in this section are shown.

### 4.1.4 Simulation scenarios

With all the geometry created, the materials assigned and the heat fluxes determined, the only critical aspect that remains to be prepared before launching the simulations is to choose when FILD is going to be measuring and when it is going to be in parking.

Two different simulation scenarios have been designed:

- A scenario where FILD stays in parking position during 30 pulses of plasma, which represents a typical working day for JT-60SA. It will serve to examine how well FILD behaves under the minimal thermal load.

- A more interesting scenario where FILD measures in certain moments and stays in parking in others. The scenario that has been designed consists on measuring during 20 seconds at the start of the plasma pulse every five plasma pulses, then hiding inside the port plug for the rest of the time. A clarifying scheme is shown in Figure 4.18.

  It is important to note that the time it takes FILD to deploy is already included in those 20 seconds, meaning that the real time FILD is measuring will actually be shorter. According to the mechanical study, the time it would take FILD to go from parking position to measuring position or vice versa is about five seconds, giving FILD more than enough time to measure, since the scintillating sensor works in frequencies in the MHz order and, therefore, just requires a few milliseconds to perform the measurements.

The main caution that has to be taken at the time of creating these scenarios in ANSYS Workbench is to activate the correct plasma heat fluxes in the correct times. All the plasma heat fluxes shall be deactivated during the 1800 s between each plasma pulse and depending on the position of FILD, whether it is the measuring position or the parking position, the corresponding plasma heat fluxes shall be activated according to the scenarios previously defined when the plasma is active.

### 4.1.5 Temperature initialization

Using APDL commands, the temperature of every body has been initialized at 100 ºC in order to decrease the time it takes for FILD to stabilize over a cyclical temperature evolution.
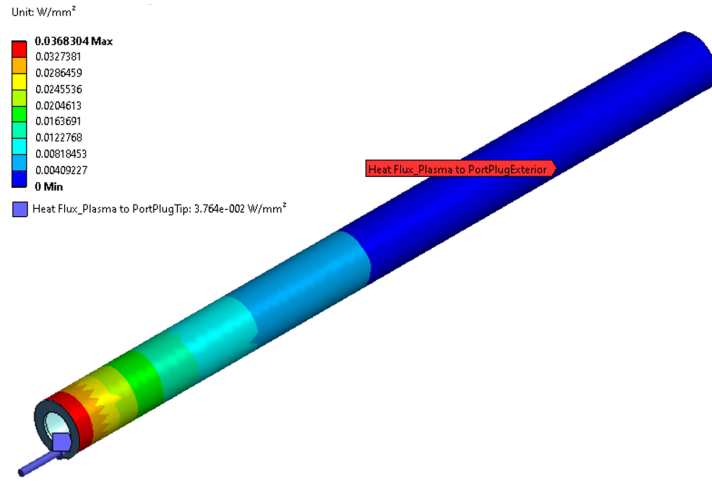
**(a)** Heat flux applied to the port plug external face and tip. Valid for both the parking and measuring position.
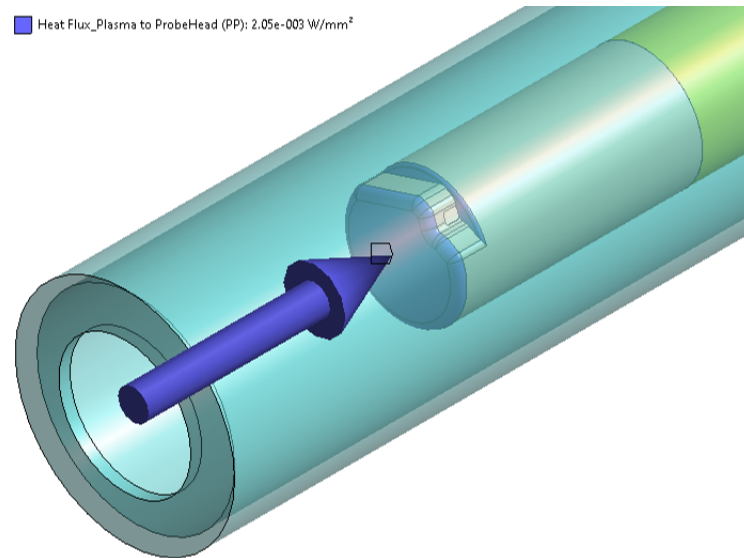


**(b)** Heat flux applied to the tip of the probe head while in parking position.
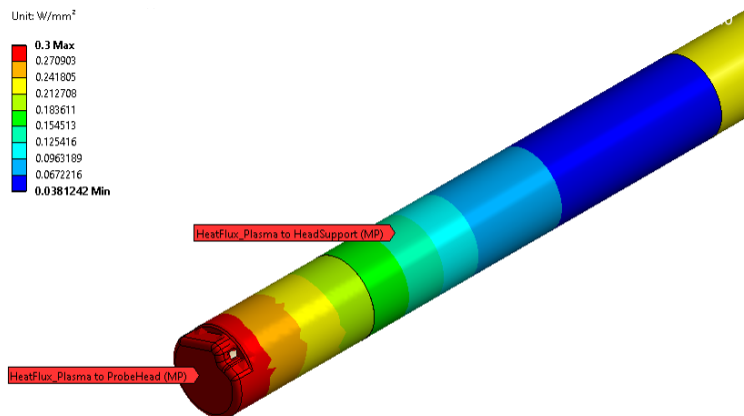


**(c)** Heat flux applied to the probe head and the portion of the head support exposed to the plasma while in measuring position.

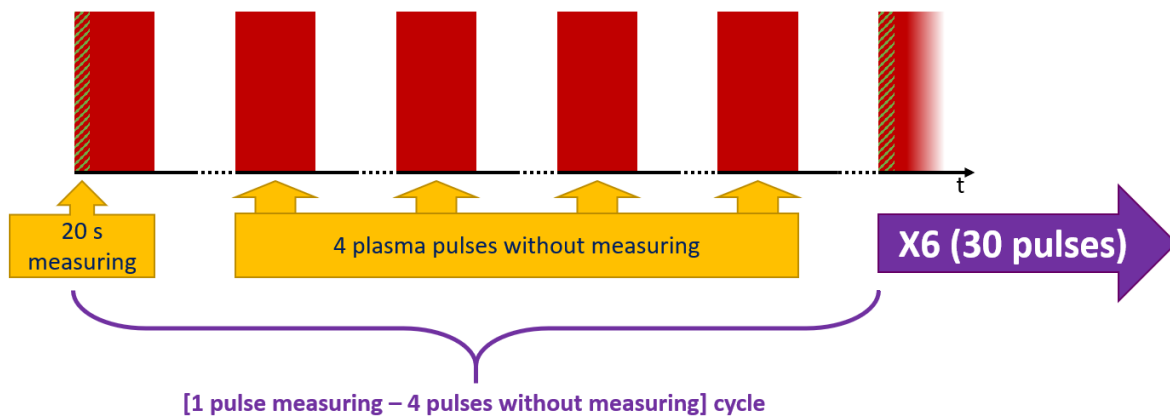**Figure 4.17**  Imposed heat fluxes due to plasma heating.

**Figure 4.18** Scheme of the '[1 pulse measuring – 4 pulses without measuring] cycle during 30 pulses' scenario.

## 4.2 Results

After running the '30 pulses in parking' scenario, the maximum temperatures of the scintillator, the probe head, the head support and the port plug have been plotted over all the time of the simulation as can be seen in Figure 5.7.
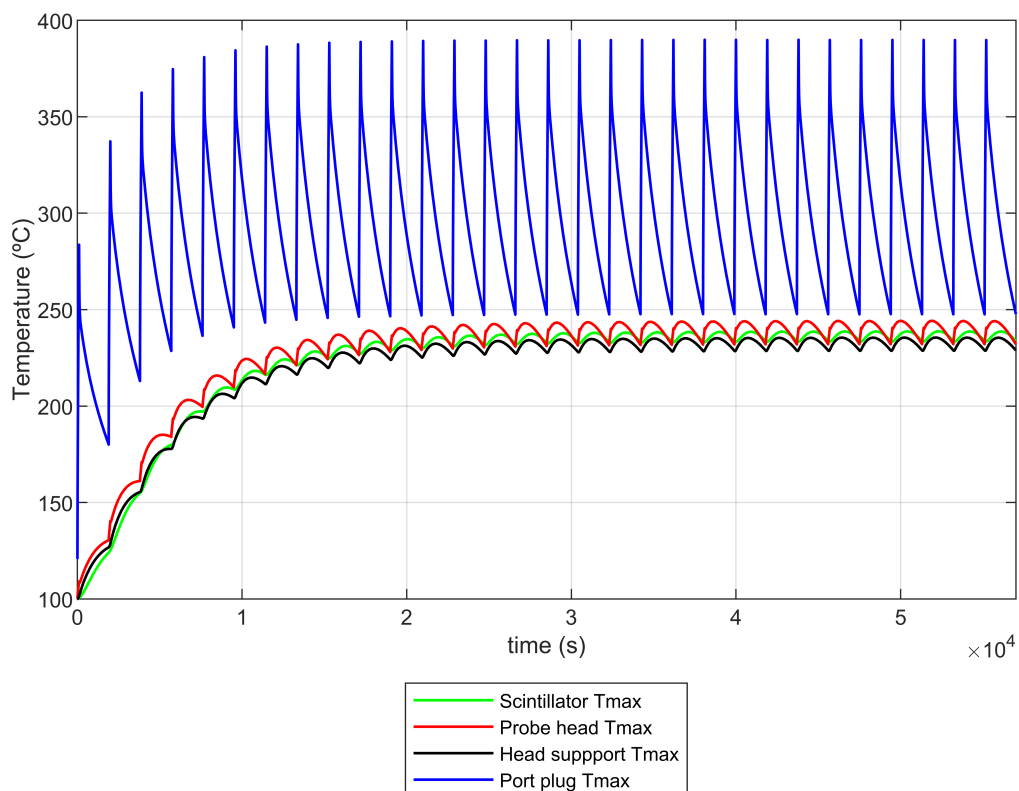


**Figure 4.19** Preliminary thermal assessment. '30 pulses in parking' scenario: Maximum temperatures over time.

From Figure 5.7, it can be observed that:

- The overall maximum temperature of the port plug is kept below 400 ºC and the head support is rather stabilized at around 230 ºC. These temperatures are always well below 1000 ºC, meaning that steel will not recrystallize.

- The maximum temperature of the probe head is kept at around 240 ºC and, therefore, very far away from the sublimation point of graphite which is located above 2000 ºC.

- Regarding the scintillator, its temperature slightly oscillates around 240 ºC, a great margin away from the 500 ºC that would result in a permanent degradation. However, its temperature never goes below 200 ºC, meaning that it cannot cool down enough even being kept all the time in parking position.

It has been proved that, in this state, FILD will never be in good condition to measure. There is no point, then, in running the '[1 pulse measuring – 4 pulses without measuring] cycle during 30 pulses' scenario, since the temperature of the scintillator can only get higher in that scenario. A solution must, therefore, be implemented and that is the purpose of the next chapter.

# 5 Final thermal assessment

In the last chapter, the objective of keeping the scintillator temperature below 200 ºC was not achieved even keeping the probe head in its parking position all the time.

Many possible solutions have been discussed like shortening the port plug (while keeping the same parking position distance), implementing an active cooling system or implementing a passive one. However, deteriorating the mechanical behaviour of FILD or risking a possible leakage of coolant into the vacuum vessel were not very attractive options. On the other hand, a passive cooling system was very interesting, although it still had to be considered how to execute it.

In the first place, the component that is going to be cooled down must be determined. We could for instance, try to cool down the port plug or the probe head and consequently reduce the temperature of the scintillator. However, there are few possibilities of cooling down these bodies since they are already connected to relatively cool surfaces, as shown in Figure 5.1, where the conductive heat transfer is dominant and therefore, very little room for improvement exists. Another option would be trying to cool down the head support, but as it was implied before, it is already cool enough in its farther from the plasma regions. The last component, and the chosen one, we could try to cool down is the scintillator. It would be the most logical approach since it is the temperature of the scintillator that is critical. In addition, the only heat transfer mechanism that has been modelled for the scintillator is radiation. Radiation is known to be a poor heat transfer mechanism when the temperature difference between bodies is relatively small, so implementing a conduction mechanism would greatly improve the temperature of the scintillator.
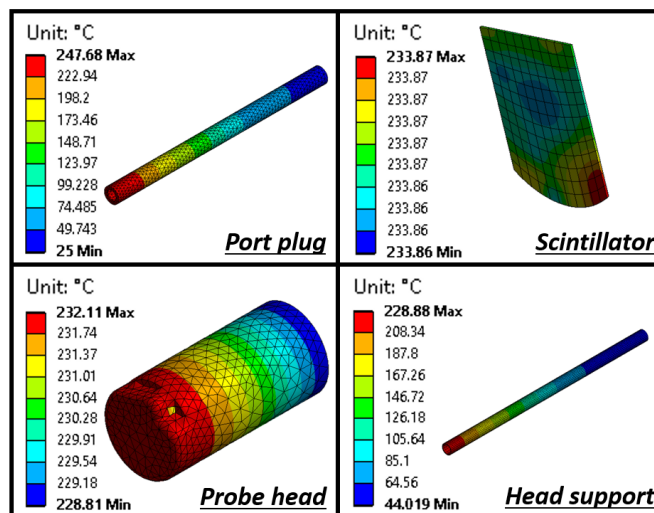


**Figure 5.1** Preliminary thermal assessment. '30 pulses in parking' scenario: Distribution of temperatures an instant before a plasma pulse.

In the second place, the element against which, the scintillator is going to be connected, must be chosen. By observing the Figure 5.1 a possible option would be to connect the scintillator to the back of the port plug, that has a temperature as low as 25 ºC, by a wire. This wire, though, should incorporate a spring or a movable part, since the scintillator changes its position when changing from parking position to measuring position and vice versa, as opposed to the port plug that has a fixed position. The chosen option, however, has been to connect the scintillator to the head support. It has the advantage that there is no need for movable parts and therefore reliability is better.

## 5.1   Thermal model upgrades

The main change for these new simulations with respect to the previous one is the new component that has been called the heat sink. It is attached to the back of the scintillator, as it can be seen in Figure 5.2 and transfers heat towards the head support through two rigid wires, appropriately disposed so they do not interfere with the light signals of the scintillator when it is impacted by fast ions. The connection with the head support, shown in Figure 5.3, has been designed as a ring where those wires can be inserted and with enough contact surface with the head support so it does not become a bottleneck for heat transfer.
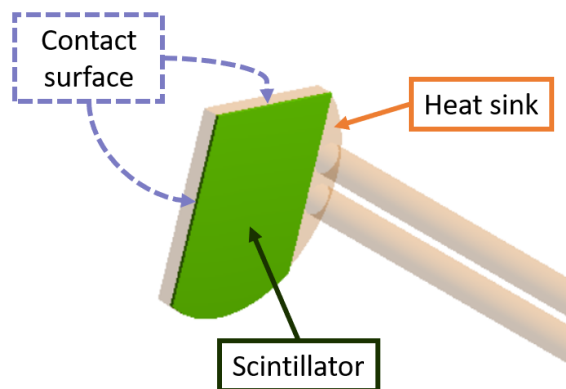


**Figure 5.2**  Connection between the heat sink and the scintillator.
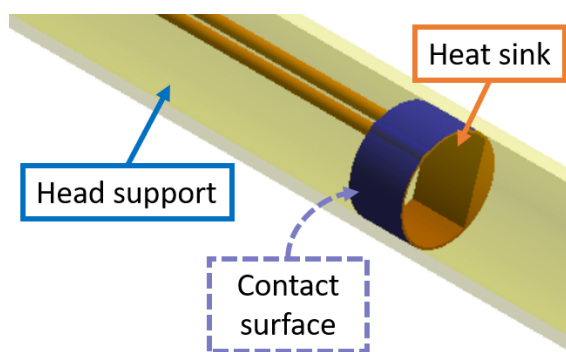


**Figure 5.3**  Connection between the heat sink and the head support.

The material assigned to the heat sink is copper due to its great thermal conductivity. The properties for this material are the default ones that can be found in Ansys Workbench and are shown in table Table 5.1.

One of the main aspects of the heat sink that had to be designed is the length of the wires which is equivalent

**Table 5.1** Copper properties.

| Copper (default Ansys Workbench) | |
|---|---|
| Density (kg/m$^3$) | 8933 |
| Thermal conductivity (W/m°C) | 400 |
| Specific heat (J/kg°C) | 385 |

to say the position of the connection to the head support. One could think that the best position is the one with the lowest temperature, however, according to the equation of the thermal conduction for the geometry of a wire (equation (5.1)), the heat transferred not only depends on the temperature difference between the ends of the wire, but also on the distance between those ends. Therefore, the best position for this connection cannot be directly inferred.

$$q = \frac{kA}{L}(T_1 - T_2)$$ (5.1)

where

$q$ is the heat flow going from the hotter end of the wire to the cooler one

$k$ is the thermal conductivity of the wire material

$A$ is the area of the section of the wire

$L$ is the length of the wire

$T_1$ is the temperature of the hotter end of the wire

$T_2$ is the temperature of the cooler end of the wire

Before determining that position, a simplification useful for this purpose will first be done: given the difference in size between the scintillator and the head support, the equality of materials and the relatively small temperature difference between them, it can be supposed that the addition of a heat sink that extracts heat from the scintillator and transfers it to the head support does not greatly change the temperature distribution of the head support.

The temperature distribution of the head support along its distance for the instant before a new plasma pulse has been extracted from the simulation performed in chapter 4 and has been plotted in Figure 5.4.

Although the temperature distribution varies depending on the moment and the operating scenario, this one has roughly been taken as a representative sample.

With respect to the thermal conductivity, $k$, its value was already given in Table 5.1 and regarding the area of the section, it has finally be decided to model two wires instead of one to better optimize the space available. Each one of them has a diameter of 10 mm and they have a combined section area, $A$, of about 157 mm$^2$.

The troublesome remaining parameters from the equation (5.1) are $q$ and $T_1$, and we say they are troublesome since they are interdependent. The equation (5.2) shows this dependency, which is a common characteristic in this type of problem.

$$q = mc_p\Delta T$$ (5.2)

where

$q$ is the heat extracted from the scintillator.

$m$ is the mass of the scintillator.

$c_p$ is the specific heat of the scintillator material.

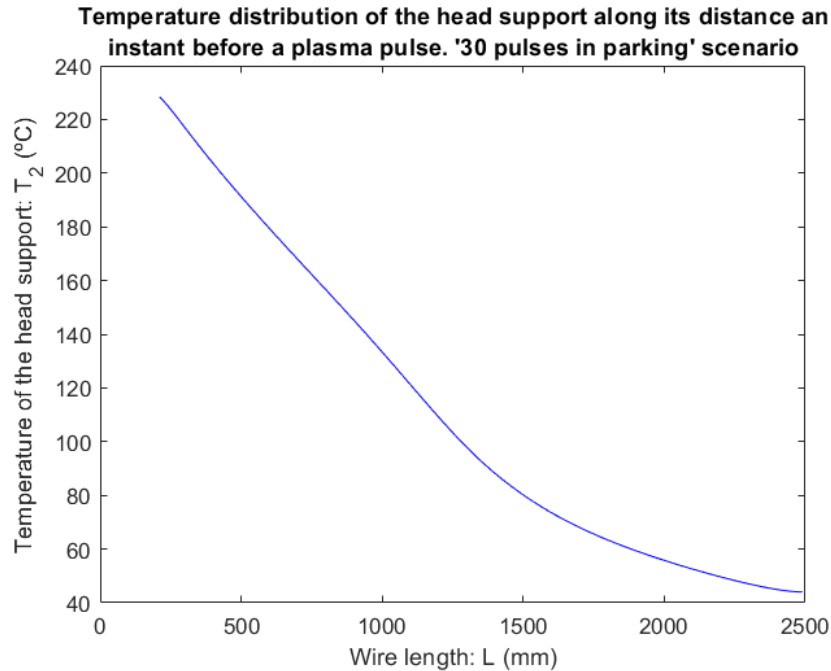$\Delta T$ is the temperature decrease of the scintillator.



**Figure 5.4** Temperature distribution of the head support along its distance an instant before a plasma pulse in the '30 pulses in parking' scenario.

Since we want to decrease the temperature of the scintillator, according to the equation (5.2), the objective is to maximize the heat extracted from the scintillator thanks to the heat sink.

The never-reaching steady state, the different possible operating scenarios, the complexity of the model and the time it takes the software to simulate those scenarios makes us unable to be strictly rigorous in the search of this optimum. The approach taken is to suppose a range of possible resulting temperatures for the scintillator and then, determine, for those temperatures, the length of the wire that gives the highest heat flow, taking into account the distribution of temperatures of the head support previously chosen as a representative sample. While not knowing the real final temperature of the scintillator, an estimate of the optimum range for the length of the wire can be obtained.

In view of the Figure 5.5, a wire length $L = 1500$ *mm* has been chosen for the following reasons:

1. The heat flux for this length is very close to the optimums when the temperature of the scintillator is between 200 ºC and 175 ºC, which is when it is critical to have a good heat extraction, since it would be near the limit of the scintillator operation (around 200 ºC).

2. The heat flux for this length is not too far from the optimum for any of the plotted temperatures of the scintillator.

3. The decrease of heat flux when the wire is longer than the optimum looks less detrimental compared to the situation where it is shorter. This is specially important in the case of an aggressive operating scenario where a temperature above 200 ºC might be reached; the heat extracted for the chosen length would be
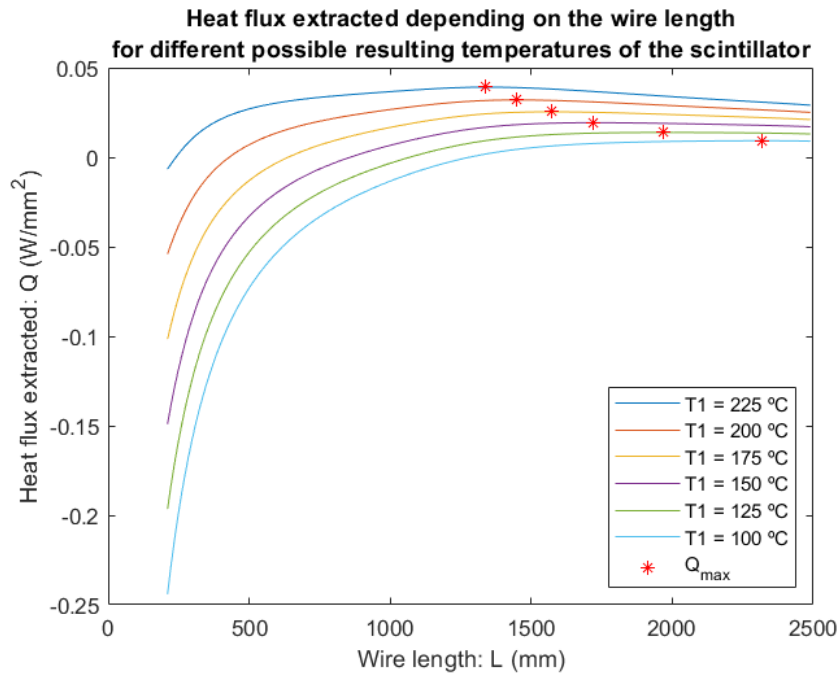
**Figure 5.5**  Heat flux extracted depending on the wire length and maximum heat flux that can be extracted for different possible resulting temperatures of the scintillator.

very close to the optimum one in that case.

The final aspect of the heat sink is shown in Figure 5.6. The ring that connects the wires to the head support has a contact area of about 140 cm$^2$ and its length is small enough not to suppose a big change in the optimization previously performed.



**Figure 5.6**  General view of the heat sink.

On another note, no emissivity has been applied to any part of the heat sink since it is planned to be insulated against every heat flux other than the conduction one. In order to achieve this, a high thermal resistivity cover has been proposed. While the cover might reach a high temperature via radiation, the heat flux towards the heat sink should remain very low.

## 5.2  Updated thermal simulations

After implementing the new changes to the model, the '30 pulses in parking' scenario simulation has been executed again and the results are shown in Figure 5.7.

It can be observed in that image, that the maximum temperature of the scintillator remains now well below 200 ºC, giving, this time, plenty of opportunities for measuring scenarios. The situation for the rest of the components remains very similar to the first simulation which was already positive.

Now that the goals have been achieved under the minimal thermal load, the '[1 pulse measuring - 4 pulses without measuring] cycle during 30 pulses' scenario can be simulated. The simulation results for this scenario are shown in Figure 5.8.
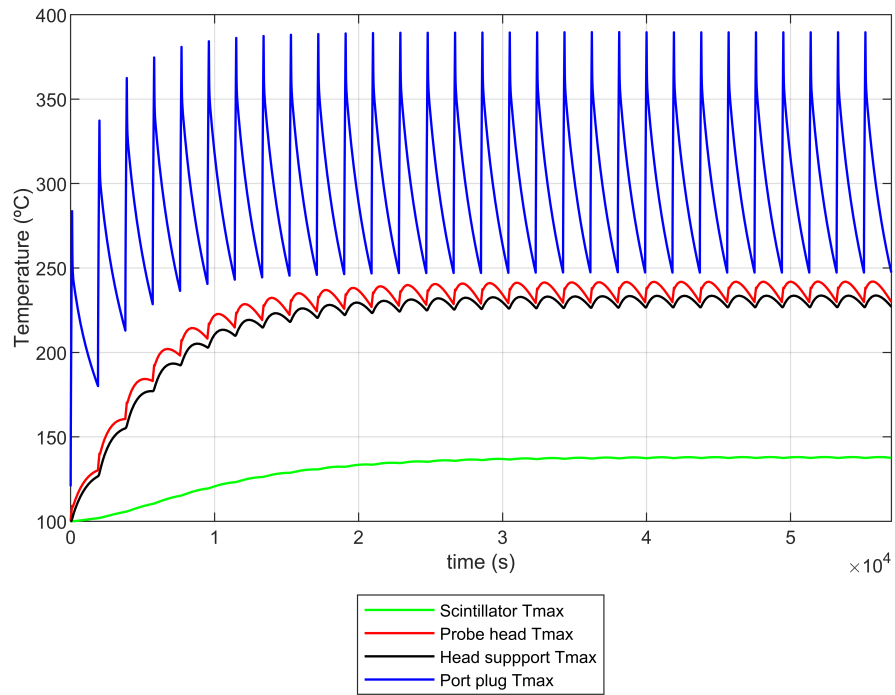
**Figure 5.7**  Final thermal assessment. '30 pulses in parking' scenario: Maximum temperatures over time.
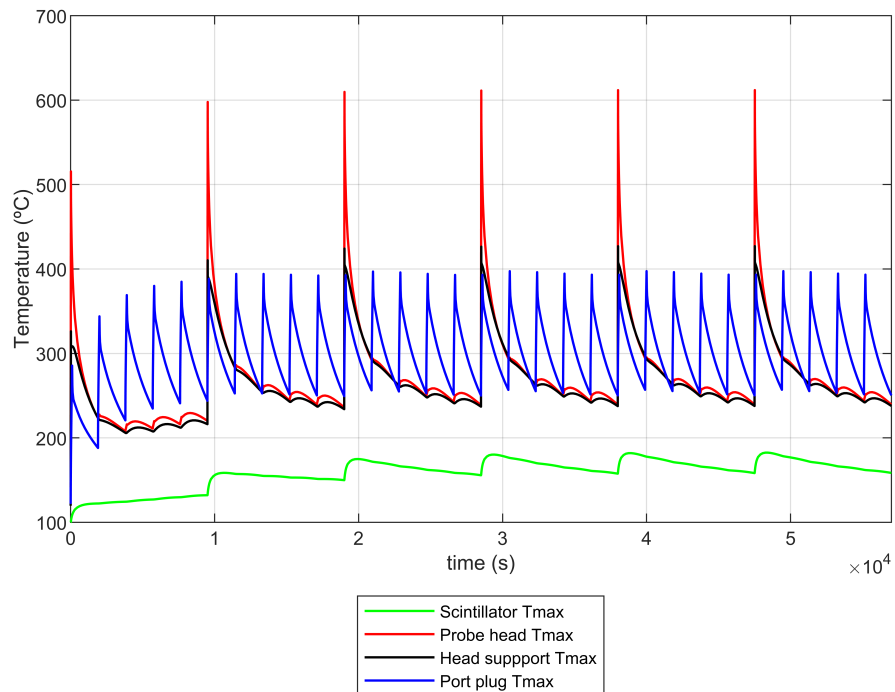


**Figure 5.8**  Final thermal assessment. '[1 pulse measuring - 4 pulses without measuring] cycle during 30 pulses' scenario: Maximum temperatures over time.

Again, the heat sink is able to keep the temperature of the scintillator below 200 ºC all the time, which was the greatest concern for this scenario. Regarding the port plug, its maximum temperature changes very little as could have been expected since the port plug receives the same amount of plasma heat flux independently of whether FILD is in parking position or in measuring position. Conversely, the probe head and the head support do notice the span of 20 seconds FILD is measuring and they experience a temperature spike. However, the probe head and the head support maximum temperatures only slightly exceed 600 ºC and 400 ºC, respectively. They are well below the critical temperatures that were 2000 ºC for the graphite probe head to sublimate and 1000 ºC for the stainless steel head support to recrystallize.

# 6  Conclusions and future work

The goals of keeping the components of FILD within an acceptable range of temperatures has been successfully accomplished for the scenarios that have been designed.

After a first unexpected setback where it was seen how the goal of keeping the temperature of the scintillator below 200 ºC was far from being achieved even after performing some optimizations, we have been able to propose and design some changes that have turned the tables. The new component, the heat sink, has proved to be a great way for cooling down the scintillator while not compromising the mechanical behaviour.

In the future, many other measuring scenarios could also be simulated like, for example, an scenario where measures are taken every plasma pulse but during shorter times since, as it was already explained in subsection 4.1.4, the current 20 seconds of measurement implemented in this work are excessive. In reality, much shorter periods of measuring will take place, instead.

Another scenario where it could be interesting to analyse the behaviour of FILD is during the baking of the tokamak. The baking of the tokamak consists on a full day process in which everything inside the tokamak is set to a temperature of about 200 ºC thanks to a series of resistances attached to the walls of the vacuum vessel. In this scenario, instead of evaluating the temperatures, it would probably be interesting to evaluate the thermal stress of the components of the JT-60SA FILD or other mechanical aspects.

Some fixes to the model should be implemented too. One of the main obstacles that has not been overcome is the impossibility to change the geometry within a same simulation in Ansys Workbench, meaning that, while the right heat fluxes have been applied in the correct moments, the physical position of the components has remained unchanged in the parking position all the time. Compared to reality, this slightly alters the simulated radiation flows while FILD should be in measuring position. However, that time span is so small compared to the whole simulation, that the changes might be very subtle.

Optimizations in this work have been mainly done "by hand". Nevertheless, Ansys Workbench has certain utilities that help the user to find the best choices by running multiple simulations in what is called design of experiments. It was recently mentioned, in chapter 5, the difficulty of finding the best length of the heat sink wire for reducing the temperature of the scintillator. This could be rather easy to do thanks to the design of experiments. Same could be applied to the parking position distance. The downside of this feature is the insane amount of time it could take Ansys Workbench to perform it, specially when models grow increasingly complex. It has been considered unnecessary to use that feature for our model except for some little tests, not shown in this work, where every aspect of the model had to simplified.

Finally, it might be decided, in a future, to add to the model other components which already exist in the more complex CAD model and that have been considered superfluous for this work.

# List of Figures

# List of Tables

# Bibliography

[1] "Final energy consumption by sector and fuel in Europe — European Environment Agency." [Online]. Available: https://www.eea.europa.eu/data-and-maps/indicators/final-energy-consumption-by-sector-10/assessment (Accessed 2020-10-08).

[2] "Renewable energy statistics - Statistics Explained." [Online]. Available: https://ec.europa.eu/eurostat/statistics-explained/index.php/Renewable_energy_statistics#Share_of_renewable_energy_almost_doubled_between_2004_and_2018 (Accessed 2020-10-08).

[3] "Renewable Energy Challenges." [Online]. Available: https://www.esrl.noaa.gov/gsd/renewable/challenges.html (Accessed 2020-10-08).

[4] "Energy - Our World in Data." [Online]. Available: https://ourworldindata.org/energy#energy-consumption-by-source (Accessed 2020-10-25).

[5] B. Bigot, "ITER, vers la maîtrise de l'énergie des étoiles," 2019.

[6] "Nuclear fusion - Wikipedia." [Online]. Available: https://en.wikipedia.org/wiki/Nuclear_fusion (Accessed 2020-09-23).

[7] "Nuclear binding energy | physics | Britannica." [Online]. Available: https://www.britannica.com/science/nuclear-binding-energy (Accessed 2020-09-23).

[8] Y. K. Bae, R. J. Beuhler, Y. Y. Chu, G. Friedlander, and L. Friedman, "DD nuclear-fusion reactions with small D2O and H2O clusters impacting heavy ice," *Physical Review A*, vol. 48, no. 6, pp. 4461–4466, 1993.

[9] R. Onofrio, "Concepts for a Deuterium-Deuterium Fusion Reactor 1," *Journal of Experimental and Theoretical Physics*, vol. 127, no. 5, pp. 883–888, 2018.

[10] "Timeline of nuclear fusion - Wikipedia." [Online]. Available: https://en.wikipedia.org/wiki/Timeline_of_nuclear_fusion (Accessed 2020-10-15).

[11] "Fusion reactor - Principles of magnetic confinement | Britannica." [Online]. Available: https://www.britannica.com/technology/fusion-reactor/Principles-of-magnetic-confinement (Accessed 2020-11-22).

[12] G. D. Dubus, *From plain visualisation to vibration sensing: using a camera to control the flexibilities in the ITER remote handling equipment*, 2014, no. January.

[13] "Research at JET- EUROfusion." [Online]. Available: https://www.euro-fusion.org/index.php?id=134&L=454%27A%3D0 (Accessed 2020-10-20).

[14] "JT-60SA Design." [Online]. Available: http://www.jt60sa.org/b/index_nav_3.htm?n3/index.htm (Accessed 2020-10-21).

[15] "Proposals | Max-Planck-Institut für Plasmaphysik." [Online]. Available: https://www.ipp.mpg.de/4144445/proposals (Accessed 2020-11-22).

[16] "Tracking the fast ion." [Online]. Available: https://www.iter.org/newsline/102/1396 (Accessed 2020-10-20).

[17] C. Fusion, "Velocity-space sensitivity and tomography of scintillator-based fast-ion loss detectors Preprint of Paper to be submitted for publication in," no. 633053, 2018.

[18] J. Ayllon-guerola, C. Cobacho-rodriguez, J. Segado-fernandez, and J. Hidalgo-salaverri, "Thermo-mechanical Assessment of the JT-60SA Fast-Ion Loss Detector."

[19] E. R. G. Eckert, "Radiative transfer, H. C. Hottel and A. F. Sarofim, McGraw-Hill Book Company, New York, 1967. 52 pages," *AIChE Journal*, vol. 15, no. 5, pp. 794–796, sep 1969. [Online]. Available: http://doi.wiley.com/10.1002/aic.690150504

[20] D. D. Incropera.F.P, *Fundamentals of heat and mass transfer 6th edition*, 2015.

[21] S. Ishida, "Integration Document ( PID )."

[22] A. Mancini, "Thermal assessment of the JT-60SA Fast Ion Loss Detector (FILD)."

[23] "ANSYSimport - File Exchange - MATLAB Central." [Online]. Available: https://es.mathworks.com/matlabcentral/fileexchange/66659-ansysimport (Accessed 2020-11-02).